Fall 2013

Quantum phase transitions in impurity models and percolating lattices

Manal M. Al-Ali

Department: Physics

QUANTUM PHASE TRANSITIONS IN IMPURITY MODELS AND PERCOLATING LATTICES

by

MANAL M. AL-ALI

A DISSERTATION

Presented to the Faculty of the Graduate School of the

MISSOURI UNIVERSITY OF SCIENCE AND TECHNOLOGY

In Partial Fulfillment of the Requirements for the Degree

DOCTOR OF PHILOSOPHY

in

PHYSICS

2013

Approved by

Dr. Thomas Vojta, Advisor
Dr. Gerald Wilemski
Dr. Paul Parris
Dr. Julia Medvedeva
Dr. Adrian Del Maestro

PUBLICATION DISSERTATION OPTION

This dissertation contains two parts, a general introduction (Section 1) and preprints of two research papers (Papers I-II) that have already been published as well as one manuscript (Paper III). The introductory chapter is written in normal dissertation style. Paper I is published in Phys. Rev. B **84**, 195136, 2011. Paper II is published in Phys. Rev. B **86**, 075119, 2012. All articles are written in the style (REVTEX4) of the American Physical Society.

ABSTRACT

This thesis investigates the influence of random disorder and dissipation on zero-temperature quantum phase transitions. Both phenomena can fundamentally change the character of the phases of a quantum many-particle system and of the transitions between them. If dissipation and disorder occur simultaneously in a system undergoing a quantum phase transition, particularly strong effects can be expected.

In the first paper reproduced in this thesis, we study a single quantum rotor coupled to a sub-Ohmic dissipative bath. We find that this system undergoes a quantum phase transition from a delocalized phase to a localized phase as the dissipation strength is increased. We determine the exact critical behavior of this transition; it agrees with that of the corresponding long-range interacting classical model. Therefore, the quantum-to-classical mapping is valid for the sub-Ohmic rotor model.

In the second paper, we investigate the influence of sub-Ohmic dissipation on randomly diluted quantum Ising and rotor models. We find that the zero-temperature quantum phase transition across the lattice percolation threshold separates an unusual super-paramagnetic cluster phase from an inhomogeneous ferromagnetic phase. We determine the low-temperature thermodynamic behavior in both phases, and we relate our results to the smeared transition scenario for disordered quantum phase transitions.

In the last paper, the influence of Ohmic dissipation on the random transverse-field Ising chain is studied by means of large-scale Monte-Carlo simulations. Our simulations show that Ohmic dissipation destroys the infinite-randomness quantum critical point of the dissipationless system. Instead, the quantum phase transition between the paramagnetic and ferromagnetic phases is smeared, as predicted by a recent strong-disorder renormalization group approach.

To my father, the cresset lighting my way.

To my soulful mother.

To my supportive husband.

ACKNOWLEDGMENTS

First and foremost, I would like to give my thanks to my advisor Dr. Thomas Vojta for his great interest in my work and his assistance in the pursuit of these studies and the preparation of this thesis.

I wish to thank my committee members, Dr. Gerald Wilemski, Dr. Paul Parris, Dr. Julia Medvedeva, and Dr. Adrian Del Maestro for their input, valuable discussions and accessibility.

I would also like to thank our department chairman, Dr. George D. Waddill, and his staff: Ellen Marie Kindle, Pamela J. Crabtree, Janice Gargus and Russell L. Summers for all their help.

I am heartily thankful to my brothers and sisters in law for their support and encouragement, especially my brother Abdulrazzaq, whose words gave me a great meaning of life.

I would like to thank my sister Um Mohammad for her encouragement.

My thanks are also give to all my friends in Jordan and USA.

I would like to express my eternal appreciation towards my father and mother who have always been there for me no matter where I am, for all their encouragement and patience.

Finally, a great thank you to, my husband, Abu Yusuf for help and support.

TABLE OF CONTENTS

Page

LIST OF ILLUSTRATIONS

LIST OF TABLES

1. INTRODUCTION

1.1 PHASE TRANSITIONS

Phase transitions are qualitative changes of the properties of a thermodynamical system as some external parameter (control parameter) varies. In classical phase transitions, which take place at nonzero temperature, the phase transition is driven by thermal fluctuations which cause the system to go from one energy configuration to another. Figure 1.1 gives an example: Decreasing the temperature of a ferromagnetic material takes it from the paramagnetic phase to the ferromagnetic phase at the critical temperature T_c (the transition point). However, phase transitions can also be reached by varying a non-thermal control parameter such as magnetic field, pressure and chemical dilution at the absolute zero of temperature. These transitions are driven by the so-called quantum fluctuations which, in principle, stem from Heisenberg's uncertainty principle. The kind of phase transitions that occur at zero temperature when a non-thermal control parameter varies is called quantum phase transition. Quantum phase transitions as well as classical transitions can be classified according to the continuity or discontinuity of the free energy derivatives as either first-order and second-order transitions. In first-order phase transitions, a first derivative of the free energy is discontinuous. These transitions are distinguished by latent heat and phase coexistence on the phase boundary (as, for example, the ice-to-water phase transition). On the other hand, second-order phase transitions (also known as continuous phase transitions) are distinguished by continuous first derivatives of the free energy while higher derivatives show divergences at the transition point. Quantum phase transitions have attracted considerable attention in the last two decades; they have become one of the most active research areas in both theoretical and experimental condensed matter physics [1, 2, 3, 4, 5].

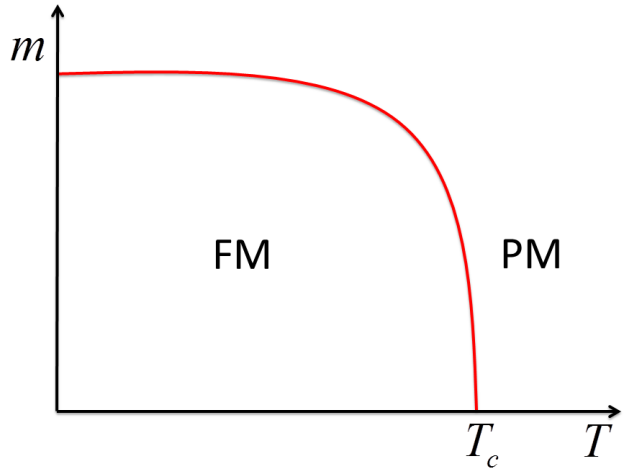

Figure 1.1: Schematic of a ferromagnetic phase transition. If the temperature T is larger than the Curie temperature T_c, the spontaneous magnetization m vanishes. For $T < T_c$, the material has a nonzero m. Thus, T_c separates the ferromagnetic (FM) and paramagnetic (PM) phases.

1.1.1. Order Parameter and Landau Theory . Modern theories of phase transitions are mostly built on the so-called Landau theory [6, 7, 8, 9]. Landau suggested that for a given phase transition the free energy F_L (known as Landau free energy) should fulfil two requirements: It has to be an analytic function of the *order parameter* m and this function must obey the symmetries of the Hamiltonian of the phase transition problem. The order parameter is a macroscopic thermodynamic quantity that vanishes in the disordered phase and develops a non-zero value in the ordered phase. For instance, for a ferromagnetic system undergoing a phase transition, the order parameter is the average magnetization which has the value zero in the paramagnetic phase and a non-zero value in the ferromagnetic phase, see figure 1.1.

Because Landau assumed that the free energy is an analytic function of the order parameter, phase transitions can be explained by expanding the free energy F_L in a power series of the order parameter m as

$$F_L(m) = F_0 + rm^2 + vm^3 + um^4 + \mathcal{O}(m^5) - hm \tag{1.1}$$

where r, v, u are parameters that are independent of the order parameter m but depend on all other degrees of freedom (such as temperature, pressure, etc.). h is an external field. F_0 denotes the nonsingular (back ground) contribution to the free energy. According to Landau, the physical order parameter m is the one that minimizes F_L. If the system is invariant under the symmetry transformation ($m \to -m$), the coefficients of the odd powers of m must vanish.

Let us discuss $F_L(m)$ for zero external field $h \to 0$: If $r > 0$, the minimum of the free energy is located at $m = 0$ whereas if $r < 0$, the minimum free energy is found at $m \neq 0$. Thus, we have a phase transition from $m = 0$ (disordered phase) to $m \neq 0$ (ordered phase) at $r = 0$. In other words, r measures the distance to the phase transition point.

If the cubic coefficient $v \neq 0$, the transition at $r = 0$ occurs discontinuously, i.e., Landau theory describes a first-order phase transition. If $v = 0$ (as is often the case by symmetry) the transition occurs continuously. The theory then describes a second-order phase transition, and $r = 0$ is the critical point. In this case, the order parameter vanishes as $m = \pm(-r/2u)^{1/2}$, when the critical point is approached from the ordered phase ($r < 0$). Thus, Landau theory predicts the order parameter singularity $m \sim |r|^\beta$ at the critical point, where the critical exponent has the mean field value $\beta = 1/2$. This is an example of the so-called super-universality of Landau theory. The values of critical exponents predicted by Landau theory for all phase transitions are identical to the usual mean-field values. The singularity of other observables can be found analogously. The definitions of the commonly used critical exponents and their mean-field values are given in table 1.1.

Table 1.2 gives the actual critical exponents of the Ising model for different dimensions ($d = 2, 3, 4$). One can immediately notice that for $d = 2$ and $d = 3$, the critical exponents deviate from the prediction of Landau theory in table 1.1 and agree with it for $d = 4$. This suggests a breakdown of Landau theory for the Ising model in $d = 2$ and 3. The reason for the failure of Landau theory to describe the critical

Table 1.1: Critical exponents within (Landau) mean-field theory. The definitions are: Specific heat $c \propto |r|^{-\alpha}$, order parameter $m \propto (-r)^{\beta}$, susceptibility $\chi \propto |r|^{-\gamma}$, external field $h \propto |m|^{\delta}\mathrm{sign(m)}$, correlation function $G(x) \propto |x|^{-d+2-\eta}$, and correlation length $\xi \propto |r|^{-\nu}$.

critical exponent	α	β	γ	δ	η	ν
quantity	c	m	χ	h	$G(x)$	ξ
mean-field value	0	1/2	1	3	0	1/2

behavior is that it does not include the fluctuations of the order parameter about its average.

The effects of the fluctuations of the order parameter depends on the systems dimensionality d and on the number of the order parameter components n, where the fluctuations decreases with increasing d and n. This introduces two different critical dimensions into the problem, the upper critical dimension d_c^+ and the lower critical dimension d_c^-.

For d larger than d_c^+, order parameter fluctuations about its average value are unimportant which implies that Landau theory provides the correct description of critical behavior. Below the lower critical dimension d_c^-, fluctuations are very strong, therefore they completely destroy the long-range order and no phase transition is observed. If d is between the upper and lower critical dimensions ($d_c^+ > d > d_c^-$), a phase transition exists but the order parameter fluctuations are sufficiently strong to

Table 1.2: Critical exponents of (2-4)-dimensional Ising model.

critical exponent	α	β	γ	δ	η	ν
2-dimensional [10]	0	1/8	7/4	15	1/4	1
3-dimensional [11, 12]	0.104	0.325	1.2385	5.2	0.039	0.632
4-dimensional	0	1/2	1	3	0	1/2

lead to a critical behavior different from Landau theory predictions. Thus, another theory is needed that includes the fluctuations.

To include the fluctuations, one can generalize the Landau free energy to the Landau-Ginzburg-Wilson free energy functional,

$$F_{LGW} = \int d^d x [F_L(\phi(x)) + |\nabla\phi(x)|^2] \tag{1.2}$$

where $\phi(x)$ is a fluctuating position-dependent field whose average value equals the order parameter, $m = \langle\phi(x)\rangle$. The second term in equation (1.2) punishes spatial order parameter variations. In a ferromagnet, this term corresponds to the domain wall energy.

The partition function can be found by integrating over all possible fluctuations in $\phi(x)$ which leads to the functional integral

$$Z_{LGW} = \int D[\phi(x)] e^{-F_{LGW}}. \tag{1.3}$$

1.1.2. The Scaling Hypothesis and Universality. The scaling theory of critical points was put forward on a heuristic basis before it became analytically derivable by means of the renormalization group theory [13, 14, 15]. It builds on the idea of long-range correlations. To be precise, the correlation function of the order parameter fluctuations $G(x) = \langle\phi(x)\phi(0)\rangle$ becomes long-ranged when the critical point is approached from the disordered phase and the typical length scale (correlation length ξ) diverges as the distance from the critical point r vanishes,

$$\xi \sim r^{-\nu}. \tag{1.4}$$

This suggests that the correlation length is the only relevant length scale in the system at the critical point [16]. Therefore, the thermodynamic properties must be invariant under a rescaling of all lengths by a positive length scale factor b while the external

parameters are adjusted such that the correlation length retains its old value. Thus, if all lengths are scaled by a factor b, the distance from criticality r and the field h can be rescaled as $r_b = rb^{y_r}$ and $h_b = hb^{y_h}$. This leads to a homogeneity relation for the free energy density $f = -(k_B T/V)\ln(Z)$ that reads

$$f(r,h) = b^{-d} f(rb^{y_r}, hb^{y_h}). \tag{1.5}$$

where y_r and y_h are critical exponents. Under the same transformation the correlation length is rescaled as

$$\xi(r,h) = b\xi(rb^{y_r}, hb^{y_h}). \tag{1.6}$$

As the scaling factor b is arbitrary, we can choose it as $b = r^{-1/y_r}$. Using this in the free energy (1.5) and correlation length (1.6) leads to the scaling forms

$$f(r,h) = r^{d/y_r} F(\frac{h}{r^{\nu y_h}}) \tag{1.7}$$

and

$$\xi(r,h) = r^{-1/y_r} A(\frac{h}{r^{\nu y_h}}) \tag{1.8}$$

where F and A are scaling functions that depend on the combination $hr^{-\nu y_h}$ only.

Setting the magnetic field to zero in (1.8) shows that the correlation length diverges as

$$\xi \sim |r|^{-1/y_r} \sim |r|^{-\nu}, \tag{1.9}$$

which implies that y_r is the inverse correlation length exponent, $y_r = 1/\nu$.

Moreover, taking appropriate derivatives of $f(r,h)$ gives analogous homogeneity relations for other thermodynamic quantities such as the magnetization

$$m(r,h) = r^{(d-y_h)\nu} M\left(\frac{h}{r^{\nu y_h}}\right). \tag{1.10}$$

At zero field $h = 0$, the magnetization can be written as $m(r) \sim r^{(d-y_h)\nu} \sim r^{\beta}$ where $\beta = (d - y_h)\nu$. Similarly, at the critical point ($r = 0$), the choice of $b = h^{-1/h_h}$ yields $m \sim h^{(\frac{d-y_h}{y_h})} \sim h^{\frac{1}{\delta}}$ giving Widom's scaling relation $\delta = \frac{y_h}{d-y_h}$.

In addition, the magnetic susceptibility as a function of r and h can be derived as

$$\chi(r, h) = r^{-(2y_h-d)\nu} X\left(\frac{h}{r^{\nu y_h}}\right) \tag{1.11}$$

where $\chi(r, h = 0) \sim r^{-(2y_h-d)\nu} X(0) \sim r^{-\gamma}$ gives the so-called Fisher's scaling law $\delta = (2y_h - d)\nu$. Similarly, the specific heat is given by $C(r) \sim r^{\nu d-2} \sim r^{-\alpha}$ leading to Josephson's scaling relation $\alpha = 2 - \nu d$.

Scaling theory thus shows that the critical exponents are not all independent from each other. Rather they are related by the scaling laws which can be summarized as

$$\delta - 1 = \frac{\delta}{\beta}, \qquad \text{Widom}'\text{s Identity} \tag{1.12}$$

$$2\beta - \gamma + \alpha = 2, \qquad \text{Rushbook}'\text{s Identity} \tag{1.13}$$

$$\nu(2 - \eta) = \gamma, \qquad \text{Fisher}'\text{s Identity} \tag{1.14}$$

$$2 - \alpha = d\nu. \qquad \text{Josephson}'\text{s Identity} \tag{1.15}$$

The last relation (also known as hyperscaling relation) contains a dependence on the dimensionality d. It is only valid below the upper critical dimension d_c^+. For $d > d_c^+$, the critical behavior is governed by the mean field theory, and therefore the critical exponents are independent of the dimensionality.

The critical exponents display a remarkable phenomenon: they are the same for entire classes of phase transitions occurring in different physical systems. This phenomenon is called the universality and the corresponding classes of systems are called the universality classes. These classes are determined only by symmetries of

the Hamiltonian and the spatial dimensionality of the system. The universality phenomenon can be understood near the critical point because the correlation length diverges. The system thus effectively averages over large volumes such that the microscopic details become unimportant.

1.1.3. Quantum Phase Transition. Quantum phase transitions are zero-temperature phase transitions that can be reached by varying an external non-thermal parameter such as magnetic field, pressure or chemical composition. This class of phase transition was first investigated by Hertz [17] in 1976. He started from the dependence of the critical temperature T_c of a given phase transition on the non-thermal parameters mentioned above. In some systems, the critical temperature can be suppressed without limit leading to $T_c = 0$ as is shown in the schematic phase diagram in figure 1.2.

By increasing the non-thermal parameter g, the classical critical temperature T_c decreases continuously. At g_c, the critical temperature reaches zero. At this point, the macroscopic order can only be destroyed by nonthermal fluctuations, i.e., quantum fluctuations which stem from Heisenberg's uncertainty principle. The critical point associated with a continuous quantum phase transition is called the quantum critical point.

Since the absolute zero of temperature cannot be attained in experiment, quantum phase transitions may seem as an abstract theoretical idea. However, a wide variety of experiments can be explained by them because the quantum fluctuations dominate the critical properties of a material not just at absolute zero temperature but also in the vicinity of the quantum critical point. For example, in a metallic system, the presence of a quantum critical point causes non-Fermi liquid behavior, i.e., unusual power-law temperature dependencies observed at experimentally attainable temperatures [18, 19].

The basic phenomenology of a second-order quantum phase transition is similar to that of a second-order classical transition. The spatial correlations of the order

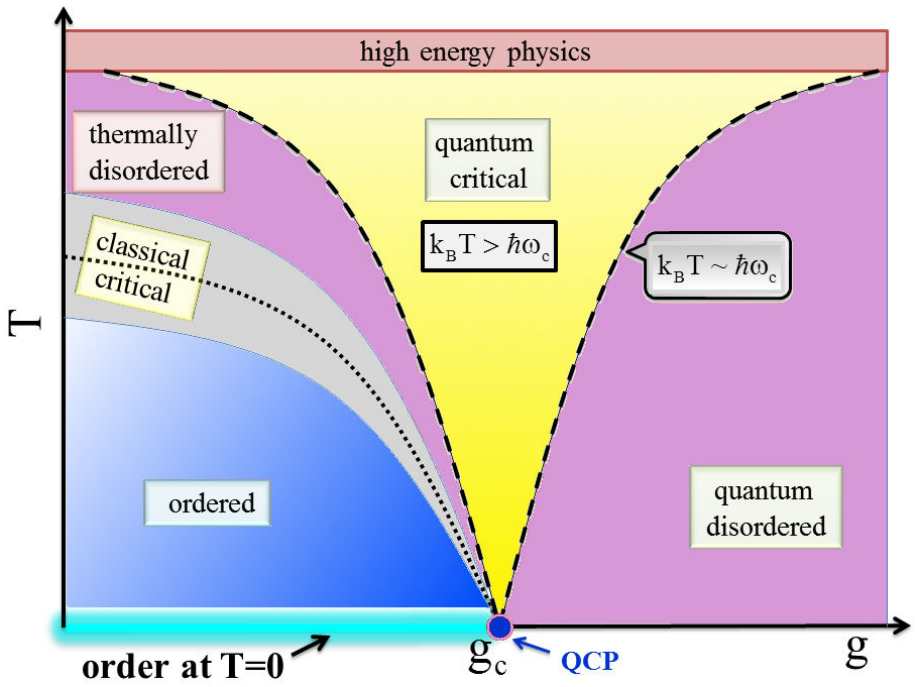

Figure 1.2: Schematic phase diagram in the vicinity of a quantum critical point (QCP). The dotted line is the finite-temperature phase boundary while the dashed lines are crossover lines separating different regions within the disordered phase. g stands for one of the possible nonthermal parameters that tune the quantum phase transition.

parameter fluctuations become long-range as the critical point is approached, and their typical length scale ξ (the correlation length) diverges as $\xi \sim |r|^{-\nu}$, where r is some dimensionless distance from the quantum critical point $r = (g - g_c)/g_c$ and ν is the correlation length critical exponent. Analogously, the typical time scale ξ_τ (correlation time) for a decay of the correlations diverges as $\xi_\tau \sim \xi^z \sim |r|^{-z\nu}$ at the quantum critical point where z is the dynamical critical exponent. Correspondingly, the typical frequency scale ω_c and the typical energy scale $\hbar\omega_c \sim |r|^{z\nu}$ go to zero.

The question under what conditions the quantum phase transition is important for an experiment can be answered by distinguishing fluctuations with predominantly thermal and quantum character. At absolute zero-temperature (no thermal fluctuations), the transition is driven by quantum fluctuations and completely controlled by quantum physics. If the transition occurs at finite temperature, quantum fluctuations

are important as long as $\hbar\omega_c > k_B T$, where $k_B T$ is the thermal energy and $\hbar\omega_c$ is the quantum energy scale. On other hand, quantum fluctuations become unimportant for $\hbar\omega_c < k_B T$ or $|t| \lesssim T_c^{1/(z\nu)}$, where $t = \frac{T-T_c}{T_c}$. Correspondingly, the asymptotic critical behavior at any nonzero T is described by classical theory.

In the schematic phase diagram shown in Fig. 1.2, the disordered phase at finite temperature T can be divided into different regions. For low T and $r > 0$ ($g > g_c$), quantum mechanics is important and long-range order destroyed by quantum fluctuations. Thus, the region is called "quantum disordered". For magnetic transitions in metallic materials, this region is the usual Fermi-liquid region. For $T > T_c$ and $r < 0$ ($g < g_c$), the order is destroyed by thermal fluctuations and the region is called "thermally disordered".

In the classical critical region, the phase transition takes place at a finite temperature and the thermal fluctuations dominate. Thus, this region is described by the classical theory. Moreover, the quantum energy scale is less than the thermal energy ($\hbar\omega_c < k_B T$) and although quantum fluctuations are present at microscopic levels, they don't control the critical behavior.

In the quantum critical region [20] which is located near g_c but at relatively high temperature and bounded by crossover lines $(g - g_c) \sim T_c^{\frac{1}{z\nu}}$, the quantum critical ground state is excited by increasing the temperature which leads to unusual power-law temperature dependencies of observables.

In classical statistical mechanics, the static and dynamic behaviors decouple. The partition function can be factorized, since the kinetic and potential parts of the Hamiltonian ($H = H_{kin} + H_{pot}$) commute, as

$$Z = \int \prod_i dp_i e^{-\beta H_{kin}} \int \prod_i dq_i e^{-\beta H_{pot}} = Z_{kin} Z_{pot}. \tag{1.16}$$

The contribution of the kinetic part to the free energy is usually derived from a simple Gaussian integral and thus will not display any singularity. Therefore, the

classical transition can be studied using a time independent Landau-Ginzburg-Wilson theory such as Eqn (1.2). In contrast, in the quantum Hamiltonian the potential and kinetic terms in general do not commute. Thus, the partition function does not factorize, $Z \neq Z_{kin}Z_{pot}$. However, the canonical probability operator e^{-H/k_bT} can be reformulated to look like a time evolution operator in imaginary time τ. The Landau-Ginzburg-Wilson theory can then be written in terms of space and time dependent fields. An example of a quantum Landau-Ginzburg-Wilson functional has a from [17, 21]

$$S[\phi] = \int_0^\beta d\tau \int d^dx[(\partial_\tau\phi(x,\tau))^2 + (\nabla\phi(x,\tau))^2 + r\phi^2(x,\tau) + \frac{1}{2}\phi^4(x,\tau)]. \qquad (1.17)$$

Here, τ is the imaginary time given by $\tau = \frac{-it}{\hbar}$ where t denotes the real time $\beta = \frac{1}{k_BT}$, and $\phi(x,\tau)$ is the order parameter field at position x and imaginary time τ.

At non-zero temperature, the extension of the extra imaginary time dimension is finite. Close to the critical point where $\xi_\tau > \beta$, the extra dimension cannot affect the critical behavior. At $T = 0$, the imaginary time direction will extend to infinity and the imaginary time acts as an additional spatial dimension. Thus, the behavior can described by a theory in a higher dimension. Using the fact that the length and time scales are related by the dynamical exponent as $\xi_\tau \sim \xi^z$, one can generalize the scaling relation (1.5) to the case of a quantum phase transition as

$$f(r,h) = b^{-(d+z)}f(rb^{1/\nu}, hb^{y_h}). \qquad (1.18)$$

Comparing equation (1.5) and equation (1.18) explicitly shows that quantum phase transitions in d-dimension are equivalent to $(d+z)$-dimensional classical phase transitions. This is the general concept of the so-called quantum-to-classical mapping. If the space and imaginary time enter the theory symmetrically, the dynamical exponent will be $z = 1$, but in general it can be larger than one.

Let us explore the quantum-to-classical mapping in more detail. As we know, the kinetic and the potential energy parts in the quantum Hamiltonian do not commute, and the canonical quantum partition function Z does not directly factorize into kinetic and potential terms. The quantum-to-classical mapping relies on factorizing the partition function by using the Trotter decomposition [22, 23] as follows

$$Z = Tre^{-\frac{-H}{k_B T}} = \lim_{N\to\infty} Z^{(N)} \tag{1.19}$$

where $Z^(N)$ is the N-approximant of the partition function given by

$$Z^{(N)} = Tr[e^{-\beta H/N}]^N = Tr[e^{-\Delta\tau H}]^N \tag{1.20}$$

where $\Delta\tau = \frac{\beta}{N}$ and $\beta = \frac{1}{k_B T}$.

The commutator of $\Delta\tau H_{kin}$ and $\Delta\tau H_{pot}$ is of higher order in $\Delta\tau$,

$$[\Delta\tau H_{kin}, \Delta\tau H_{pot}] = (\Delta\tau)^2 [H_{kin}, H_{pot}] \approx 0. \tag{1.21}$$

Using the Trotter decomposition ($e^{A+B} = e^A e^B e^{-\frac{1}{2}[A,B]}$), and the result of equation (1.21), we can thus factorize the N-approximant of the partition function as

$$Z^{(N)} = Tr[e^{-\Delta\tau H_{kin}} e^{-\Delta\tau H_{pot}}]^N. \tag{1.22}$$

By inserting N complete sets of eigenstates for the H_{kin} terms, the partition function can be written as

$$Z^{(N)} = \lim_{N\to\infty} \sum_{\{\alpha_{j,n}\}} \prod_{n=1}^{N} e^{-\Delta\tau H_{kin}(\alpha_j)} \left\langle \{\alpha_j\}_n \left| e^{-\Delta\tau H_{pot}(\alpha_j)} \right| \{\alpha_j\}_{n+1} \right\rangle. \tag{1.23}$$

where n is the index of the imaginary time slice. To get the classical Hamiltonian of the system, we need to evaluate the off-diagonal terms.

If we apply the method, for example, to the transverse-field Ising model

$$H = -\sum_{<i,j>} J_{ij} S_i^z S_j^z - \sum_i h_i S_i^x, \tag{1.24}$$

we find its equivalent classical Hamiltonian as

$$H_{class} = -\sum_{\langle i,j\rangle,n} \tilde{J}_{ij} S_{i,n}^z S_{j,n}^z - \sum_{i,n} \tilde{k}_i^\tau S_{i,n}^z S_{i,n+1}^z \tag{1.25}$$

where $\tilde{J}_{ij} = \beta J_{ij}/N$ and $\tilde{k}_i = \ln\sqrt{\coth(\beta h_i/N)}$ are the effective couplings in the space and imaginary time directions, respectively.

1.2 IMPURITY QUANTUM PHASE TRANSITIONS

Impurity quantum phase transitions are a class of quantum phase transitions occurring in systems which consist, for example, of a single spin coupled to infinite bosonic or fermionic baths. These bosons or fermions can be either real particles, quasiparticles, or collective excitations. Impurity quantum phase transitions are a realization of boundary critical phenomena at zero temperature at which only degrees of freedom of a finite-size (zero-dimensional) subsystem (e.g., the single spin) become critical at the transition point, while the rest of the system (the bath) does not undergo a transition, (but it will affect the critical behavior of the impurity).

In general, all impurity models have the form

$$H = H_{imp} + H_b + H_{imp,b}. \tag{1.26}$$

Here, H_{imp} contains the impurity degrees of freedom, and H_b contains bulk (bath) degrees of freedom. The last term $H_{imp,b}$, contains the coupling between the impurity and the bath and thus the dissipation strength. The competition between the first term H_{imp} and the last term $H_{imp,b}$ is responsible for the quantum phase transition.

Impurity quantum phase transitions of systems of the form (1.26) require the thermodynamic limit in the bath system H_b before the $T \to 0$ limit is taken. The anisotropic Kondo model [24, 25] and the pseudogap Kondo model [26] are some examples of impurity models with fermionic baths that display a quantum phase transition.

The simplest realization of an impurity system involving bosonic baths is the dissipative two-level system, also called the spin-boson model [27, 28]. It describes a two-level system coupled to an infinite bath of harmonic oscillators represented by a Hamiltonian

$$H_{SB} = -\Delta_0 \sigma_x + \epsilon \sigma_z + \sum_i \omega_i a_i^\dagger a_i + \sigma_z \sum_i \lambda_i (a_i + a_i^\dagger). \tag{1.27}$$

The spin tunnels between up $|\uparrow\rangle$ and down $|\downarrow\rangle$ states with tunneling frequency Δ_0, and is damped by the coupling to the oscillators bath. The last term in (1.27) represents the coupling between the spin and the displacement of the bath oscillators. It is completely specified by the bath spectral function

$$J(\omega) = \pi \sum_i \lambda_i^2 \delta(\omega - \omega_i). \tag{1.28}$$

Of a particular interest are power-law spectra, $J(\omega) = 2\pi\alpha\omega_c^{(1-s)}\omega^s$ with $\omega < \omega_c$, where ω_c is a cut-off frequency and α characterizes the dissipation strength. The ground state phase diagram of the system depends on the behavior of the bath spectral function for small frequency ω.

For $s > 1$, the case of so-called super-Ohmic dissipation, the damping is qualitatively weak. The spin will therefore remain in the delocalized phase for any dissipation strength α. In the case of $0 < s < 1$ (sub-Ohmic dissipation), the system will undergo a continuous quantum phase transition from a delocalized phase (Fig. 1.3a) to a localized phase (Fig. 1.3b) as the dissipation strengthen increases [29]. The marginal case ($s = 1$) corresponds to the well-studied Ohmic spin-boson model. This

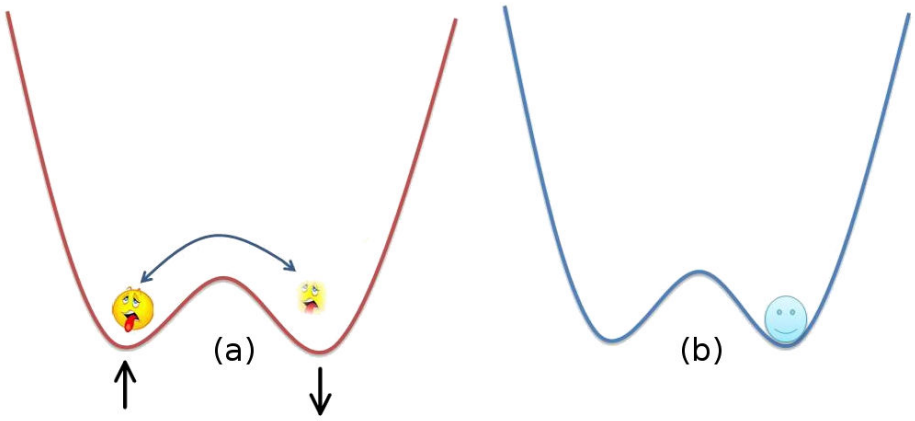

Figure 1.3: Dissipative two level system. (a) In the delocalized phase, the spin tunnels between $\uparrow$ and $\downarrow$. (b) In the localized phase, the spin ceases tunnelling and $\langle \sigma_z \rangle \neq 0$.

system shows a Kosterlitz-Thouless quantum transition [27, 28] between the localized and delocalized phases at a critical value of the dissipation strength.

Spin-boson and other dissipative impurity models have many applications in different fields such as glass physics, damping in electric circuits, and electron transfer in biological molecules. Moreover, in the context of quantum computation, the spin-boson model can be used for modeling the coupling of qubits to a noisy environment and the associated decoherence processes.

1.3 QUENCHED DISORDER EFFECTS

A real material often contains disorder, for example, lattice defects or impurity atoms. Thus many investigations focus on phase transitions in the presence of disorder [30, 31]. We concentrate in this work on disorder that does not evolve with time, also called quenched disorder or time-independent disorder, in contrast to annealed disorder, which fluctuates on short time scales. The quenched disorder is further assumed to have no qualitative effect on the two bulk phases. It only affects the phase transition point by locally shifting the tendency towards one or the other

phase. This kind of quenched disorder is referred to as weak disorder, or random-T_c disorder. It can be realized in a ferromagnetic material for example by randomly replacing magnetic atoms with nonmagnetic ones.

Such random-T_c disorder can be modeled in a LGW theory by making the bare distance from the critical point a random function of spatial position, $r \to r_0 + \delta r(x)$. In the presence of disorder in a d-dimensional lattice, the LGW theory reads

$$F_{LGW} = \int d^d x [|\nabla\phi(x)|^2 + (r_0 + \delta r(x))\phi^2(x) + u\phi^4(x) - h\phi(x)] \tag{1.29}$$

In equation (1.29), the character of the disorder is encoded in the statistical properties of the random-T_c term $\delta r(x)$. As long as the physics is dominated by long-wavelength properties and the average behavior of the disorder, the details of the probability distribution of the disorder should not play an important role. It can thus be replaced a Gaussian distribution which can be easily handled mathematically.

The presence of weak quenched disorder in a system undergoing a phase transition leads to the following questions:

- Will the transition remain sharp or it will be destroyed by smearing?
- Will the order of the transition change (first-order vs. second-order)?
- If the transition remains sharp and second-order, will the critical behavior change quantitatively (different universality class with new critical exponents) or even qualitatively (exotic non-power-law scaling)?
- Does the disorder only affect the transition itself or also the behavior in its vicinity?

Studying these questions has a long history (see reference [32] for some historical details).

1.3.1. Harris Criterion. Initially it was thought that disorder destroys sharp phase transitions because, in the presence of disorder, the system will be divided up into spatial regions which undergo the transition at different temperatures. Thus there would not be a sharp singularity in observables. However, it was found later that phase transition can remain sharp in the presence of disorder, at least for classical systems with short-range disorder correlations.

Harris [33] found a condition under which weak disorder does not affect the stability of a clean critical point of a classical phase transition. The same condition was later found to be applicable to quantum critical points. He considers a system with quenched disorder undergoing a second order phase transition at a temperature T_c. The system is divided into blocks of volume $V = \xi^d$ [34]. Each block i behaves independently and has its own effective local critical temperature T_c^i which is determined by the average of $r + \delta(x)$ over the volume of the blocks, see figure 1.4. If the standard deviation Δr of these local critical temperatures from block to block is smaller than the global distance from the critical point r, the order-parameter fluctuations caused by the weak disorder are suppressed at the transition point, and the sharp phase transition remains. The standard deviation Δr can be found using the central limit theorem as $\Delta r \sim \xi^{-d/2}$. Since the correlation length is related to r via $\xi \sim |T - T_c|^{-\nu} = r^{-\nu}$, Δr can be written as

$$\Delta r \sim r^{\frac{d\nu}{2}}. \tag{1.30}$$

Thus, a clean critical point is perturbatively stable, for $r \to 0$, if the clean critical exponents fulfill the inequality $r^{d\nu/2} < r$ or

$$d\nu > 2. \tag{1.31}$$

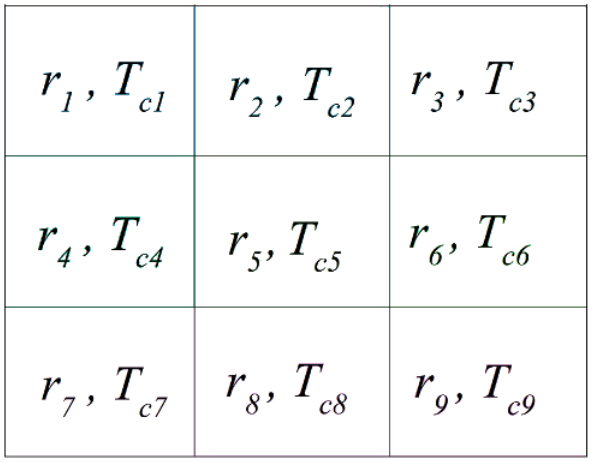

Figure 1.4: Schematic depiction of the system fragmentation used in the derivation of the Harris criterion.

This inequality is called the Harris criterion. If $\Delta r > r$, different parts of the system are in different phases, and a sharp phase transition is impossible.

Note that the Harris criterion only deals with the average behavior of the disorder at large length scales while potential new phenomena at finite length scales are not covered by it.

Based on the Harris criterion, the behavior of the disorder strength with increasing length scale, i.e., under coarse graining, can be used to classify critical points with quenched disorder [30, 31, 35]:

i- The Harris criterion is fulfilled ($d\nu > 2$). At these phase transitions, the disorder strength decreases under coarse graining and the system becomes asymptotically homogeneous at large length scales. Consequently, the critical behavior of the dirty system is identical to that of the clean system. An example of this class is the three-dimensions classical Heisenberg model with $\nu \approx 0.698$ for both clean and dirty cases [36].

If the Harris criterion is violated, the clean critical point is destabilized by weak quenched disorder, and the behavior must change. However, a sharp critical

point can still exist in the presence of the disorder. The two following classes must be distinguished.

ii- The relative disorder strength approaches a finite value, and the system remains inhomogeneous at large length scales. The phase transition stays sharp and features power-law scaling but with new critical exponents, i.e., the quenched disorder changes the universality class of the system (quantitative changes). The three-dimensional Ising model is an example of this class. The clean $\nu \approx 0.627$ violates the Harris criterion [37] and the dirty system has a value of $\nu \approx 0.684$ [38]. Note that the dirty critical exponent satisfies the Harris inequality.

iii- The relative disorder strength increases without limit under coarse graining. The new critical point is called an infinite-randomness critical point [35, 39, 40]. At this point, the power-law scaling is replaced by activated (exponential) scaling. The quenched disorder thus changes the phase transition qualitatively.

This class was first found in two-dimensional Ising model with disorder perfectly correlated in one dimension [41, 42] or equivalently in the one-dimensional random quantum Ising model [40].

The macroscopic observables of an infinite-randomness critical point have extremely broad probability distributions whose widths diverge with system size. Accordingly, the averages of the observables are dominated by rare events (spatial regions with atypical disorder configurations).

1.3.2. Smearing of Phase Transitions by Disorder. The term smeared phase transition simply describes a transition where the disorder destroys the sharp singularity of the free energy because different spatial regions order independently. This effect of disorder can be reached in both classical [43, 44, 45] and quantum systems [46, 47, 48].

In classical systems, the disorder can smear the sharp transition if it is perfectly correlated in a sufficient number of dimensions. Specifically, the dimensionality of the

defects must be larger than the lower critical dimension, $d_{RR} > d_c^-$. For example, the randomly layered Ising model (planer defects) has disorder dimensionality $d_{RR} = 2$ greater than the lower critical dimensionality of Ising symmetry $d_c^- = 1$ [43, 44, 45]. Individual layers can therefore order independently and the global transition is smeared. On the other hand, the same layered system but with Heisenberg spin symmetry has $d_c^- = 2$ resulting in a sharp phase transition with an infinite-randomness critical point. In this case, the rare regions can not statically order.

In case of quantum systems, quantum-to-classical mapping leads to $(d+1)$-dimensional classical systems where the extra dimension is related to the *imaginary time*. Quenched disorder is time invariant, thus it is perfectly correlated in the time direction. This strong correlation dramatically increases the effects of rare regions. For example, the quantum-to-classical mapping of the one dimensional random quantum Ising model (1.24) leads to a two dimensional random classical system with perfectly correlated disorder in the new time direction [41]. The phase transition of this classical system was expected to be smeared, but Fisher showed it to be sharp with an infinite-randomness critical point.

The effects of disorder are further enhanced if the order parameter fluctuations are damped by the coupling to other degrees of freedom. This can be achieved, for example by coupling each spin of the transverse-field Ising model (1.24) to a bath of harmonic oscillators,

$$H = H_{Ising} + \sum_{i,n} \left[\nu_{i,n} a_{i,n}^\dagger a_{i,n} + \frac{1}{2} \lambda_{i,n} \sigma_i^z (a_{i,n}^\dagger + a_{i,n}) \right] \tag{1.32}$$

where H_{Ising} is the Hamiltonian (1.24), the first term in the brackets is the bath Hamiltonian where $a_{i,n}(a_{i,n}^\dagger)$ is the annihilation (creation) operator of the nth oscillator coupled to spin i. The second term in the brackets is the coupling of the lattice spins to the heat bath where $\lambda_{i,n}$ is the coupling constant. The system can thus be viewed as a chain of coupled spin-boson models. Let us assume (as in Sec. 1.2) the

bath spectral functions have power law form $J(\omega) = \frac{\pi}{2}\alpha\omega_c^{1-\sigma}\omega^\sigma$. By integrating out the bath degrees of freedom in the partition function in favor of the order parameter field $\phi = \langle\sigma^z\rangle$, one can obtain a $(d+1)$-dimensional Landau-Ginzburg-Wilson (LGW) order parameter field theory. In the absence of disorder, the action is given by

$$S = \int d\tau \int d^d\mathbf{r} \left[\Gamma(\mathbf{r},\tau)\phi^2(\mathbf{r},\tau) + u\phi^4(\mathbf{r},\tau)\right] \tag{1.33}$$

where $\Gamma(\mathbf{r},\tau)$ is the bare Gaussian vertex. Its Fourier transform has the structure (prefactors suppressed)

$$\Gamma(\mathbf{q},\omega_n) = r + \mathbf{q}^2 + |\omega_n|^\sigma. \tag{1.34}$$

Here, r is the bare distance from criticality, and the dynamic term proportional to $|\omega_n|$ stems from the damping of the order parameter fluctuations by the bath. On the other hand, for undamped dynamics the leading term is the ω_n^2 term. The disorder appears in the coefficients of the action such as the distance from criticality, i.e., r becomes a function of spatial position as $r \to r_0 + \delta r(x)$, and thus the action now contains random-T_c disorder (weak disorder).

The effect of the damping can be seen by performing quantum-to-classical mapping of the full Hamiltonian (1.32) and integrating out the bath degree of freedom to obtain the Hamiltonian of a classical lattice spin system.

$$H = -\frac{1}{2}\sum_{i,\{\tau,\tau'\}} \frac{\tilde{\alpha}_i}{|\tau-\tau'|^{1+\sigma}} S_{i,\tau}S_{i,\tau'} - \frac{1}{2}\sum_{\tau,<i,j>} \tilde{J}_{ij}S_{i,\tau}S_{j,\tau} \tag{1.35}$$

where $S_{i,\tau} = \pm 1$ and $< i,j >$ represents the nearest-neighbor interactions in the space direction, $\{\tau,\tau'\}$ represents the long-range interactions in the time direction, and $\sigma = 1$ for the Ohmic damping case ($\sigma < 1$ for the sub-Ohmic case and $\sigma > 1$ for the super-Ohmic case). The Ising chain with long-range $1/r^2$ interaction is known to have an ordered phase [49, 50, 51]. Therefore, sufficiently large but finite-size rare regions of the Hamiltonian (1.35) can independently undergo the phase transition

and develop true static order while the bulk phase is paramagnetic. Thus, the global order develops gradually and the global phase transition is smeared.

The same scenario also applies to magnetic quantum phase transitions in disordered metals. Hertz [17] derived order parameter field theories of these transitions by integrating out the fermionic degrees of freedom. They take the same form as given in equation (1.33) and (1.34). In this case the Ohmic damping stems from the coupling of the order parameter to fermionic particle-hole excitations.

1.4 PERCOLATING LATTICE

1.4.1. Percolation Theory. In coffee makers, percolation represents the flow of the coffee through porous media from top to bottom. In mathematics and physics it refers to the geometry of lattice models of random systems and the nature of the connectivity in them.

Let us consider a d-dimensional hypercubic lattice with bonds between the nearest neighbor sites. Each site in the lattice is occupied at random with probability p, or empty with probability $(1-p)$. Moreover, the sites are assumed to be independent. [This problem is called "site percolation"]. In a slightly different mathematical model, a bond is closed with probability p or open with probability $(1-p)$ [the corresponding problem is called "bond percolation"]. In both cases, each group of two or more occupied (connected) neighboring sites is called a cluster.

Now, the question is: What is the probability to have a large occupied cluster that spans the entire lattice [from top to bottom] for a given occupation probability p? In the thermodynamic limit, such a cluster is known as the infinite cluster. By Kolmogorov's zero-one law [52], for a given p, the probability that an infinite cluster exists is either zero or one in the thermodynamics limit. For a small occupation probability p, there is only a very tiny chance of having a large cluster. This chance will be increased if p becomes larger and larger, and for p close to one we almost

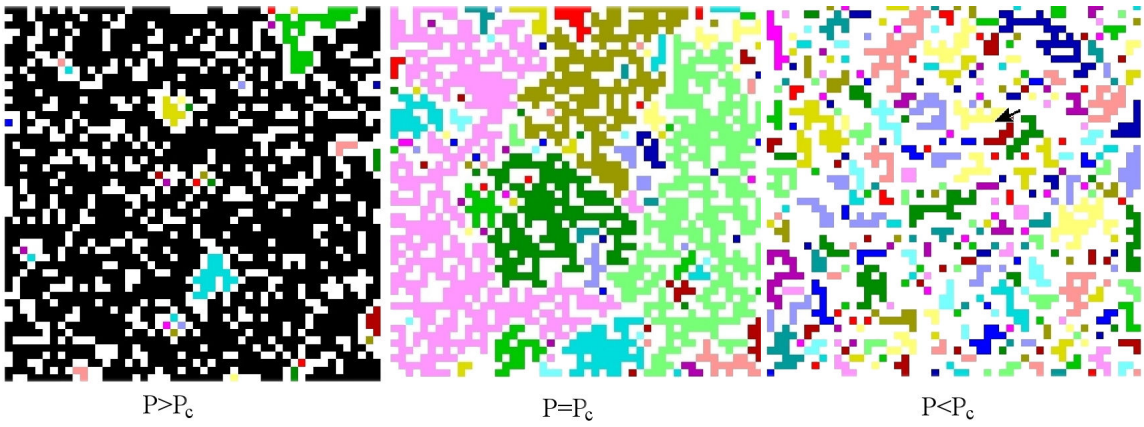

Figure 1.5: Snapshot of diluted system at different occupation probability p. Different colors represents different clusters.

certainly will have a cluster percolating through the lattice. Thus, the probability of having that infinite cluster is an increasing function of p, and (due to Kolmogorov's law) there must be a some value of p below which the probability is always zero and above which the probability is always one. This value of p is called the percolation threshold or the critical occupation probability denoted by p_c.

This suggests that the lattice can be in one of two "phases", separated by a sharp transition at the percolation threshold ($p = p_c$). For $p > p_c$, the infinite cluster exists as will some smaller clusters, and the system will be in the connected phase (the percolating phase). In contrast, for $p < p_c$ the lattice is decomposed into small disconnected finite-size clusters only; the system will be in the disconnected phase. Right at $p = p_c$, there are clusters of all length scales, see Figure 1.5.

We can look at the geometric phase transition between these two phases as a continuous (second-order) phase transition where the geometric fluctuations due to dilution play the role of the usual thermal or quantum fluctuations. The order parameter for this transition is the probability P_∞ of a site to belong to the infinite connected percolation cluster (P_∞ also represents the number of sites in the infinite cluster per lattice site), which has zero value for $p < p_c$ (no infinite cluster exists) and

a non-zero value for $p > p_c$. Close to p_c, it varies as

$$p_\infty = \begin{cases} |p - p_c|^{\beta_c} & p > p_c \\ 0 & p < p_c \end{cases} \tag{1.36}$$

where β_c is the order parameter critical exponent of classical percolation. (Note: the subscript c will be used to distinguish the classical percolation exponents from other exponents). In addition to the infinite cluster, we also need to characterize the finite-size clusters on both sides of the percolation threshold. The typical size or correlation length ξ_c of a finite cluster diverges with the correlation length exponent ν_c

$$\xi_c \sim |p - p_c|^{-\nu_c} \tag{1.37}$$

as p_c is approached. The average mass S_c (or the average number of sites) of a finite cluster takes the role of the response function (the susceptibility) in a conventional second-order phase transition, (see figure 1.6). It diverges with the susceptibility exponent γ_c according to

$$S_c \sim |p - p_c|^{\gamma_c}. \tag{1.38}$$

A central quantity is the cluster size distribution n_s, which contains the complete information about the percolation critical behavior. n_s defines the number of finite size clusters with s sites per lattice site, and it is normalized by the total number of lattice sites to ensure that it is independent of the lattice size. Close to p_c, it obeys the scaling form

$$n_s(p) = s^{-\tau_c} f[(p - p_c)s^{\sigma_c}] \tag{1.39}$$

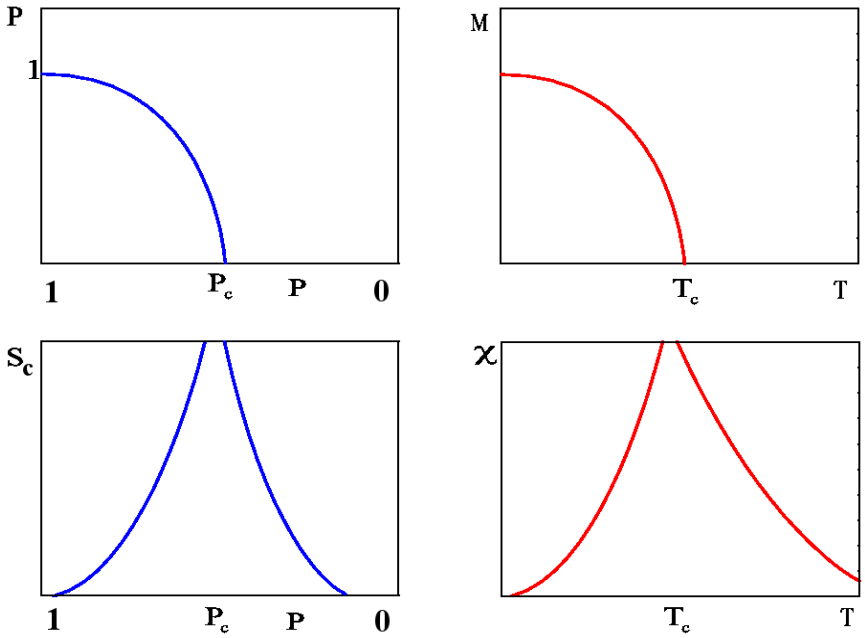

Figure 1.6: Percolation as a critical phenomena. This figure compares the percolation transition to a ferromagnetic critical point. The probability of a site to be in the infinite cluster P_∞ and the average cluster size S_c in the geometric transition take the roles of magnetization m and susceptibility χ in the classical ferromagnetic to paramagnetic transition, respectively.

where σ_c and τ_c are critical exponents. $f(x)$ is a scaling function which behaves as

$$\begin{aligned} f(x) &\sim \exp\left[-B_1 x^{\frac{1}{\sigma_c}}\right] && x > 0 \\ f(x) &= \text{constant} && x = 0 \\ f(x) &\sim \exp\left[-(B_2 x^{\frac{1}{\sigma_c}})^{1-\frac{1}{d}}\right] && x < 0 \end{aligned} \cdot \tag{1.40}$$

where d is the dimensionality of the system.

From the behavior of $f(x)$, one can notice that n_s takes a power law form at $p = p_c$ which means that all cluster sizes exist at the percolation threshold. For $p \gg p_c$ and $p \ll p_c$, n_s decays exponentially with s, thus large clusters are suppressed.

The classical percolation exponents are determined by τ_c and σ_c as follows: the correlation length exponent $\nu_c = \frac{\tau_c - 1}{d\sigma_c}$, the order parameter exponent $\beta_c = \frac{\tau_c - 2}{\sigma_c}$, and the susceptibility exponent $\gamma_c = \frac{3-\tau_c}{\sigma_c}$ [53].

1.4.2. Application of Percolation Theory to Thermal and Quantum Phase Transition. Imagine a magnetic system in which only a fraction p of all lattice sites is occupied by spins and the remaining fraction $(1-p)$ is left non-magnetic. The spins are distributed randomly as in the percolation problem, and neighboring spins interact via an exchange interaction J.

According to the percolation point of view the model consists of different clusters of spins. At low temperature ($k_BT << J$), the spins within one cluster will be parallel to each other. A cluster of s sites thus acts as a single effective spin (super-spin) with a moment proportional to s.

A- Diluted Ising Model at Low Temperatures. We are going to describe the behavior of a classical Ising model on a randomly diluted lattice at low temperature, where the thermal fluctuations have no effect on the critical behavior. Let us consider a site-diluted Ising model given by the Hamiltonian

$$H = -J \sum_{<i,j>} \epsilon_i \epsilon_j \sigma_i \sigma_j - h \sum_i \epsilon_i \sigma_i \tag{1.41}$$

where σ_i is a classical Ising spin at lattice site i, and $J > 0$ is the exchange interaction between nearest neighbors. Dilution is introduced via the random variable ϵ_i which can take the value one or zero with probability p and $(1 - p)$, respectively.

In the absence of dilution (i.e., $p = 1$), the model shows long-range order (ferromagnetic phase) at sufficiently low temperatures (provided $d \geq 2$). Because of the dilution, magnetic order will be weakened for $p < 1$. The question now is: What is the effect of the dilution on the ferromagnetic phase and on the phase transition to paramagnet.

For $k_BT \ll J$, a cluster of Ising spins of size s in an external symmetry-breaking field h has two possible energy configurations, all spins oriented in h direction with energy $-sh$, or in opposite direction with energy $+sh$. The magnetization of

the cluster of size s is thus given by

$$m_{cluster} = \frac{\sum_{\sigma=\pm 1} s\sigma e^{-\frac{s\sigma h}{k_B T}}}{\sum_{\sigma=\pm 1} e^{-\frac{s\sigma h}{k_B T}}} = s \tanh\left(\frac{sh}{k_B T}\right). \tag{1.42}$$

The contribution of all finite size clusters to the total magnetization would be

$$m_{finite} = \sum_s s n_s \tanh\left(\frac{sh}{k_B T}\right) \tag{1.43}$$

where n_s is the cluster size distribution (1.39). If the occupation probability $p > p_c$, an infinite cluster exists and provides a contribution of

$$m_\infty = \pm P_\infty \sim \pm |p - p_c|^{\beta_c} \tag{1.44}$$

to the total magnetization. Thus, the total magnetization is given by

$$m = m_\infty + m_{finite} = \pm P_\infty + \sum_s s n_s \tanh\left(\frac{sh}{k_B T}\right). \tag{1.45}$$

For $h \to 0$, only the infinite cluster contribution remains. The magnetization thus vanishes as $(p - p_c)^\beta$ at the percolation threshold, and the critical exponent of the magnetization is identical to the percolation order parameter exponent β_c (rather than the conventional undiluted Ising exponent).

If the occupation probability $p < p_c$, magnetic long-range order is impossible (no infinite cluster), and the system consists of independent super-spins. Thus, the low temperature behavior of sufficiently diluted Ising model is different from that of conventional Ising model which is expected to have non-zero magnetization at low temperature.

For small field h, the susceptibility ($\chi = \lim_{h\to 0} \frac{\partial m}{\partial h}$) reads

$$\chi = \sum_s \frac{s^2 n_s}{k_B T}. \tag{1.46}$$

This means, it is proportional to the average cluster size [53] $S_c \sim |p - p_c|^{-\gamma_c}$. Thus $\chi \propto |p - p_c|^{-\gamma_c}$, where γ_c is the classical percolation susceptibility exponent.

These results establish a correspondence of the infinite cluster size P_∞ to the magnetization m, of the average cluster size S_c to the susceptibility χ, and of the percolation threshold p_c to the transition temperature T_c for ferromagnetism.

B- Quantum Phase Transitions on Percolating Lattices. Now, we are going to describe a quantum phase transition on a percolating lattice which occurs at absolute zero temperature. A simple example is a randomly diluted Ising model in a transverse magnetic field [54, 55, 56, 57],

$$\hat{H} = -J \sum_{<i,j>} \epsilon_i \epsilon_j \hat{S}_i^z \hat{S}_j^z - h_x \sum_i \epsilon_i \hat{S}_i^x - h \sum_i \epsilon_i \hat{S}_i^z \tag{1.47}$$

where h_x is the transverse field that controls the quantum fluctuations, h is the symmetry breaking field. In the undiluted case ($p = 1$), for $h_x << J$, the ground state is ferromagnetically ordered while for $h_x >> J$ the long-range order is destroyed by the quantum fluctuations caused by the transverse field. The two phases are separated by a quantum phase transition at $h_x \sim J$.

In the diluted model ($p < 1$), if the transverse field h_x is sufficiently small such that the quantum fluctuations are not too strong, the spins within a cluster of size s are parallel and this cluster will act as a single effective Ising spin (whose moment is proportional to s). Its low-energy physics is thus equivalent to a two-level system.

If $p < p_c$, magnetic long-range order does not exist because the system is decomposed into non-interacting finite size clusters. Thus, the system is still in the disordered phase with a total magnetization that averages to zero, $m_{total} = 0$.

For $p > p_c$, long-range order survives on the infinite percolation cluster, while all finite size clusters do not contribute. The total magnetization will be proportional

to the number of sites in the infinite cluster,

$$m_{total} = p_\infty \sim (p - p_c)^\beta \qquad\qquad p > p_c \tag{1.48}$$

where the order parameter exponent β equals magnetically the classical geometric percolation exponent β_c. The system will be in the ordered phase. Thus the critical percolation threshold p_c separate two magnetic phases. The transition across p_c was first investigated in detail by Senthil and Sachdev [57].

Another static quantity is the magnetic correlation length ξ. For small h_x, all spins of a cluster are correlated, but the correlations cannot extend beyond the cluster size, thus

$$\xi \sim \xi_c \sim |p - p_c|^{-\nu_c}. \tag{1.49}$$

The correlation exponent ν is identical to the classical geometric one, too. However, other quantities involving quantum dynamics (like the dependence of the magnetization on the ordering field h) have non-classical behavior [57].

PAPER

I. QUANTUM PHASE TRANSITION OF THE SUB-OHMIC ROTOR MODEL

Manal Al-Ali, and Thomas Vojta

[1]*Department of Physics, Missouri University of Science & Technology, Rolla, MO 65409*

ABSTRACT*

We investigate the behavior of an N-component quantum rotor coupled to a bosonic dissipative bath having a sub-Ohmic spectral density $J(\omega) \propto \omega^s$ with $s < 1$. With increasing dissipation strength, this system undergoes a quantum phase transition from a delocalized phase to a localized phase. We determine the exact critical behavior of this transition in the large-N limit. For $1 > s > 1/2$, we find nontrivial critical behavior corresponding to an interacting renormalization group fixed point while we find mean-field behavior for $s < 1/2$. The results agree with those of the corresponding long-range interacting classical model. The quantum-to-classical mapping is therefore valid for the sub-Ohmic rotor model.

*Published in Physical Review B 84, 195136 (2011)

1. INTRODUCTION

Quantum phase transitions are abrupt changes in the ground state properties of a quantum many-particle system that occur when a non-thermal control parameter is varied.[3] In analogy to thermal phase transitions, they can be classified as either first-order or continuous transitions. Continuous quantum phase transitions, also called quantum-critical points, are characterized by large-scale temporal and spatial fluctuations that lead to unconventional behavior in systems ranging from strongly correlated electron materials to ultracold quantum gases (for reviews see, e.g., Refs. [1, 4, 5, 58, 59, 60]).

Impurity quantum phase transitions [61] are an interesting class of quantum phase transitions at which only the degrees of freedom of a finite-size (zero-dimensional) subsystem become critical at the transition point. The rest of the system (the "bath") does not undergo a transition. Impurity quantum phase transitions can occur, e.g., in systems composed of a single quantum spin coupled to an infinite fermionic or bosonic bath. Fermionic examples include the anisotropic Kondo model [62] and the pseudogap Kondo model [26].

The prototypical system involving a bosonic bath is the dissipative two-state system, [27, 28] also called the spin-boson model, which describes a two-level system coupled to a single dissipative bath of harmonic oscillators. Its ground-state phase diagram depends on the behavior of the bath spectral density $J(\omega)$ for small frequencies ω. Power-law spectra $J(\omega) \propto \omega^s$ are of particular interest. In the super-Ohmic case ($s > 1$), the system is in the delocalized (disordered) phase for any dissipation strength. In contrast, for sub-Ohmic dissipation ($0 < s < 1$), there is a continuous quantum phase transition from a delocalized phase at weak dissipation to a localized (ordered) phase at strong dissipation [29]. In the marginal Ohmic case ($s = 1$), a quantum phase transition exists, too, but it is of Kosterlitz-Thouless type [27, 28].

The sub-Ohmic spin-boson model has recently attracted considerable attention in the context of the so-called quantum-to-classical mapping. This concept relates the critical behavior of a quantum phase transition in d space dimensions to that of a classical transition in $d+1$ dimensions. The mapping is usually established by comparing the order-parameter field theories of the transitions: Imaginary time in the quantum problem plays the role of the extra dimension in the corresponding classical system. In the case of the spin-boson model, the classical counterpart is a one-dimensional Ising model with long-range interactions that decay as $1/r^{1+s}$ for large distances r. In recent years, the applicability of the quantum-to-classical mapping to the sub-Ohmic spin-boson model has been controversially discussed after numerical renormalization group results [63] suggested that its critical behavior for $s < 1/2$ deviates from that of the corresponding Ising model. While there is now strong evidence [64, 65, 66, 67] that this conclusion is incorrect and that the quantum-to-classical mapping is actually valid, the issue appears to be still not fully settled [68]. Moreover, possible failures of the quantum-to-classical mapping have also been reported for other impurity models with both Ising [69, 70, 71] and higher [72, 73] symmetries; and the precise conditions under which it is supposed to hold are not resolved.

In the present paper, we therefore investigate the large-N limit of the sub-Ohmic quantum rotor model. Analogously to the spin-boson model, this system undergoes a quantum phase transition with increasing dissipation strength from a delocalized phase to a localized phase [74, 75]. We exactly solve the critical properties of this transition. Our analysis yields nontrivial critical behavior corresponding to an interacting renormalization group fixed point for $1 > s > 1/2$, while we find mean-field behavior for $s < 1/2$. All critical exponents agree with those of the corresponding long-range interacting classical model, [76] implying that the quantum-to-classical mapping is valid.

Our paper is organized as follows. We define the sub-Ohmic rotor model in Sec. 2.. In Sec. 3., we derive its partition function; and we solve the self-consistent

large-N constraint at zero and finite temperatures as well as with and without an external field. Section 4. is devoted to a discussion of observables and the resulting critical behavior. We conclude in Sec. 4..

2. SUB-OHMIC ROTOR MODEL

A quantum rotor can be understood as a point moving on an N-dimensional hypersphere of radius $N^{1/2}$. It can be represented by an N-component vector $\mathbf{S}$ satisfying $\mathbf{S}^2 = N$. The rotor has a momentum $\mathbf{P}$; the position and momentum components fulfill the usual canonical commutation relations $[S_\alpha, P_\beta] = i\delta_{\alpha\beta}$. In the large-$N$ limit, $N \to \infty$, the hard constraint $\mathbf{S}^2 = N$ can be replaced by one for the

thermodynamic average, $\langle \mathbf{S}^2 \rangle = N$, because fluctuations of the magnitude of $\mathbf{S}$ are suppressed by the central limit theorem. The large-N quantum rotor is thus equivalent to the quantum spherical model of Ref. [77, 78] which is given by the Hamiltonian

$$H_S = \frac{1}{2}P^2 + \frac{1}{2}\omega_0^2 S^2 - h\, S + \mu(S^2 - 1)\ . \tag{1.1}$$

Here, S and P represent the position and momentum of one rotor component, μ is a Lagrange multiplier enforcing the constraint $\langle S^2 \rangle = 1$, and h is an external symmetry-breaking field.[†]

We now couple (every component of) the rotor to a bath of harmonic oscillators.[‡] In the conventional linear-coupling form, the Hamiltonian describing the bath and its coupling to S reads

$$H_B = \sum_j \left[\frac{p_j^2}{2m_j} + \frac{m_j}{2}\omega_j^2 q_j^2 + \lambda_j q_j S + \frac{\lambda_j^2}{2m_j\omega_j^2} S^2 \right], \tag{1.2}$$

with q_j, p_j, and m_j being the position, momentum, and mass of the j-th oscillator. The ω_j are the oscillator frequencies and λ_j the coupling strengths between the oscillators and S. The last term in the bracket is the usual counter term which insures that the dissipation is invariant under translations in S [27]. The coupling between

[†]For the original rotor, this corresponds to a field coupling to all components, $\mathbf{h} = h(1, 1, \ldots, 1)$. This convention is convenient because the components remain equivalent even in the presence of a field.

[‡]Equivalently, the N-component rotor is coupled to N-component oscillators.

the rotor and the bath is completely characterized by the spectral density

$$J(\omega) = \frac{\pi}{2} \sum_j \frac{\lambda_j^2}{m_j \omega_j} \delta(\omega - \omega_j) \tag{1.3}$$

which we assume to be of power-law form

$$J(\omega) = 2\pi \bar{\alpha} \omega_c^{1-s} \omega^s, \qquad (0 < \omega < \omega_c) \ . \tag{1.4}$$

Here, $\bar{\alpha}$ is the dimensionless dissipation strength and ω_c is a cutoff frequency. We will be interested mostly in the case of sub-Ohmic dissipation, $0 < s < 1$.

3. PARTITION FUNCTION AND CONSTRAINT EQUATION

3.1. PATH INTEGRAL FORMULATION. We now derive a representation of the partition function in terms of an imaginary-time functional integral. Because the sub-Ohmic rotor model $H = H_S + H_B$ is equivalent to a system of coupled harmonic oscillators (with an additional self-consistency condition), this can be done following Feynman's path integral approach [79] with position and momentum eigenstates as basis states. After integrating out the momentum variables, we arrive at the partition function

$$Z = \int D[S(\tau)]D[q_j(\tau)]\; e^{-\mathcal{A}_S - \mathcal{A}_B} \; . \tag{1.5}$$

The Euclidian action is given by

$$\mathcal{A}_S = \int_0^\beta d\tau \left[\frac{1}{2}(\dot{S}^2 + \omega_0^2 S^2) - hS + \mu(S^2 - 1)\right] \tag{1.6}$$

$$\mathcal{A}_B = \int_0^\beta d\tau \sum_j \left[\frac{m_j}{2}(\dot{q}_j^2 + \omega_j^2 q_j^2) + S\lambda_j q_j + \frac{\lambda_j^2 S^2}{2m_j\omega_j^2}\right] \tag{1.7}$$

where the dot marks the derivative with respect to imaginary time τ, and $\beta = 1/T$ is the inverse temperature.

The bath action is quadratic in the q_j, we can thus exactly integrate out the bath modes. After a Fourier transformation from imaginary time τ to Matsubara frequency ω_n, this yields $\int D[\tilde{q}_i(\omega_n)] \exp(-\mathcal{A}_B) = Z_B^0 \exp(-\mathcal{A}_B\prime)$ where Z_B^0 is the partition function of the unperturbed bath and

$$\mathcal{A}'_B = T\sum_{\omega_n}\sum_j \frac{\lambda_j^2}{2m_j}\frac{\omega_n^2}{\omega_j^2(\omega_n^2+\omega_j^2)}\tilde{S}(\omega_n)\tilde{S}(-\omega_n) \; . \tag{1.8}$$

The sum over j can be turned into an integral over the spectral density $J(\omega)$. Carrying out this integral gives

$$\mathcal{A}'_B = \frac{1}{2} T \sum_{\omega_n} \alpha \omega_c^{1-s} |\omega_n|^s \tilde{S}(\omega_n) \tilde{S}(-\omega_n) \tag{1.9}$$

with the dimensionless coupling constant $\alpha = 2\pi\bar{\alpha}\,\mathrm{cosec}(\pi s/2)$. Combining $\mathcal{A}_S$ and $\mathcal{A}'_B$ yields the effective action of the sub-Ohmic rotor model as

$$\begin{aligned} \mathcal{A}_{\text{eff}} = \quad & -\beta\mu + \frac{T}{2} \sum_{\omega_n} \left(\epsilon + \alpha \omega_c^{1-s} |\omega_n|^s \right) \tilde{S}(\omega_n) \tilde{S}(-\omega_n) \\ & -T \sum_{\omega_n} \tilde{h}(\omega_n) \tilde{S}(-\omega_n) \ , \end{aligned} \tag{1.10}$$

where $\epsilon = \omega_0^2 + 2\mu$ is the renormalized distance from quantum criticality. The ω_n^2 term in $\mathcal{A}_S$ is subleading in the limit $\omega_n \to 0$. It is thus irrelevant for the critical behavior at the quantum critical point and has been dropped. The theory then needs a cutoff for the Matsubara frequencies which we chose to be ω_c. Because the effective action is Gaussian, the partition function $Z = Z_B^0 \int D[\tilde{S}(\omega_n)] \exp(-\mathcal{A}_{\text{eff}})$ is easily evaluated. We find

$$\begin{aligned} Z = \quad & Z_B^0 \exp(\beta\mu) \prod_{\omega_n} \left[\frac{2\pi}{T(\epsilon + \alpha \omega_c^{1-s} |\omega_n|^s)} \right]^{1/2} \times \\ & \times \exp \left[\frac{T}{2} \sum_{\omega_n} \frac{\tilde{h}(\omega_n) \tilde{h}(-\omega_n)}{\epsilon + \alpha \omega_c^{1-s} |\omega_n|^s} \right] \ . \end{aligned} \tag{1.11}$$

3.2. SOLVING THE SPHERICAL CONSTRAINT. The spherical (large-N) constraint $\langle S^2 \rangle = 1$ can be easily derived from the free energy $F = -T \ln Z$ by means of the relation $0 = \partial F / \partial \mu$. In the case of a time-independent external field h with Fourier components $\tilde{h}(\omega_n) = \delta_{n,0} h/T$, this yields

$$T \sum_{\omega_n} \frac{1}{\epsilon + \alpha \omega_c^{1-s} |\omega_n|^s} + \frac{h^2}{\epsilon^2} = 1 \ . \tag{1.12}$$

We now solve this equation, which gives the renormalized distance from criticality, ϵ, as a function of the external parameters α, T, and h, in various limiting cases.

1. $T = 0$ and $h = 0$. At zero temperature, the sum over the Matsubara frequencies turns into an integral, and the constraint equation reads

$$\frac{1}{\pi}\int_0^{\omega_c} d\omega \frac{1}{\epsilon + \alpha\omega_c^{1-s}\omega^s} = 1 \ . \tag{1.13}$$

For sub-Ohmic dissipation, $s < 1$, a solution $\epsilon \geq 0$ to this equation only exists for dissipation strengths α below a critical value α_c because the integral converges at the lower bound even for $\epsilon = 0$. The value of α_c defines the location of the quantum critical point. Performing the integral for $\epsilon = 0$, we find $\alpha_c = 1/[\pi(1-s)]$. As we are interested in the critical behavior, we now solve the constraint equation for dissipation strengths close to the critical one, $\alpha \lesssim \alpha_c$. We need to distinguish two cases: $1 > s > 1/2$ and $s < 1/2$.

In the first case, the calculation can be performed by subtracting the constraint equations at α and at α_c from each other. After moving the cutoff ω_c to ∞, the resulting integral can be easily evaluated giving

$$\epsilon = \alpha\omega_c A^{s/(s-1)}(\alpha_c - \alpha)^{s/(1-s)} \qquad (s > 1/2) \ , \tag{1.14}$$

where $A = -(1/s)\,\mathrm{cosec}(\pi/s)$. In the case $s < 1/2$, eq. (1.13) can be evaluated by a straight Taylor expansion in $\alpha_c - \alpha$, resulting in

$$\epsilon = \alpha_c\omega_c B^{-1}(\alpha_c - \alpha) \qquad (s < 1/2) \ , \tag{1.15}$$

with $B = 1/[\pi(1-2s)]$. For $s < 1/2$, the functional dependence of ϵ on $\alpha_c - \alpha$ thus becomes linear, independent of s. As we will see later, this causes the transition to be of mean-field type.

For dissipation strengths above the critical value α_c, the spherical constraint can only be solved by *not* transforming the sum over the Matsubara frequencies in (1.12) into the frequency integral in (1.13). Instead, the $\omega_n = 0$ Fourier component has to be treated separately.[§] Alternatively, one can explicitly introduce a nonzero average for one of the N order parameter components (see, e.g., Ref. [3]). Both approaches are equivalent; we will follow the first route in the next subsection.

2. $T > 0$ and $h = 0$. At small but nonzero temperatures, an approximate solution of the spherical constraint (1.12) can be obtained by keeping the $\omega_n = 0$ term in the frequency sum discrete while representing all other modes in terms of an ω-integral. This gives

$$\frac{T}{\epsilon} + \frac{1}{\pi}\int_0^{\omega_c} d\omega \frac{1}{\epsilon + \alpha\omega_c^{1-s}\omega^s} = 1 \ . \tag{1.16}$$

We now solve this equation on the disordered side of the transition ($\alpha < \alpha_c$), at the critical dissipation strength α_c, and on the ordered side of the transition ($\alpha > \alpha_c$). We again need to distinguish the cases $1 > s > 1/2$ and $s < 1/2$.

In the first case, we subtract the quantum critical ($T = 0, h = 0, \alpha = \alpha_c$) constraint from (1.16). After evaluating the emerging integral, the following results are obtained in the limit $T \to 0$ and $|\alpha - \alpha_c|$ small but fixed,

$$\epsilon = \frac{\alpha}{\alpha - \alpha_c} T \qquad (\alpha > \alpha_c,\ s > 1/2) \ , \tag{1.17a}$$

$$\epsilon = A^{-s}\alpha_c\omega_c^{1-s}T^s \qquad (\alpha = \alpha_c,\ s > 1/2) \ , \tag{1.17b}$$

$$\epsilon = \epsilon_0 + \frac{\alpha}{\alpha_c - \alpha}\frac{s}{1-s}T \quad (\alpha < \alpha_c,\ s > 1/2) \ . \tag{1.17c}$$

[§]This is analogous to the usual analysis of Bose-Einstein condensation where the $\mathbf{q} = 0$ mode has to be treated separately below the condensation temperature.

Here, ϵ_0 is the zero-temperature value given in (1.14) and $A = -(1/s)\,\mathrm{cosec}(\pi/s)$ as above. For $s < 1/2$, we expand (1.16) in $\alpha - \alpha_c$ and find

$$\epsilon = \frac{\alpha}{\alpha - \alpha_c} T \qquad (\alpha > \alpha_c,\ s < 1/2)\ , \tag{1.18a}$$

$$\epsilon = B^{-1/2} \alpha_c \omega_c^{1/2} T^{1/2} \qquad (\alpha = \alpha_c,\ s < 1/2)\ , \tag{1.18b}$$

$$\epsilon = \epsilon_0 + \frac{\alpha}{\alpha_c - \alpha} T \qquad (\alpha < \alpha_c,\ s < 1/2)\ , \tag{1.18c}$$

with ϵ_0 given in (1.15) and $B = 1/[\pi(1-2s)]$ as above.

3. $T = 0$ and $h \neq 0$. At zero temperature, but in the presence of an external field, the spherical constraint reads

$$\frac{1}{\pi} \int_0^{\omega_c} d\omega \frac{1}{\epsilon + \alpha \omega_c^{1-s} \omega^s} + \frac{h^2}{\epsilon^2} = 1\ . \tag{1.19}$$

Proceeding in analogy to the last subsection, we determine the distance ϵ from criticality in the limit $h \to 0$ and $|\alpha - \alpha_c|$ small but fixed. In the case $1 > s > 1/2$, we obtain

$$\epsilon = \left(\frac{\alpha}{\alpha - \alpha_c} \right)^{1/2} h \qquad (\alpha > \alpha_c,\ s > 1/2)\ , \tag{1.20a}$$

$$\epsilon = \left(A^{-s} \alpha_c \omega_c^{1-s} h^{2s} \right)^{1/(s+1)} \qquad (\alpha = \alpha_c,\ s > 1/2)\ , \tag{1.20b}$$

$$\epsilon = \epsilon_0 + \frac{\alpha}{\alpha_c - \alpha} \frac{s}{1-s} \frac{h^2}{\epsilon_0} \qquad (\alpha < \alpha_c,\ s > 1/2)\ , \tag{1.20c}$$

where ϵ_0 is the zero-field value given in (1.14) and $A = -(1/s)\,\mathrm{cosec}(\pi/s)$ as above. For $s < 1/2$, the corresponding results read

$$\epsilon = \left(\frac{\alpha}{\alpha - \alpha_c} \right)^{1/2} h \qquad (\alpha > \alpha_c,\ s < 1/2)\ , \tag{1.21a}$$

$$\epsilon = \left(B^{-1} \alpha_c^2 \omega_c h^2 \right)^{1/3} \qquad (\alpha = \alpha_c,\ s < 1/2)\ , \tag{1.21b}$$

$$\epsilon = \epsilon_0 + \frac{\alpha}{\alpha_c - \alpha} \frac{h^2}{\epsilon_0} \qquad (\alpha < \alpha_c,\ s < 1/2)\ , \tag{1.21c}$$

with ϵ_0 given in (1.15) and $B = 1/[\pi(1-2s)]$ as above.

4. OBSERVABLES AT THE QUANTUM PHASE TRANSITION

After having solved the spherical constraint, we now turn to the behavior of observables at the quantum critical point.

4.1. MAGNETIZATION. The magnetization $M = \langle S \rangle$ follows from (1.11) via $M = -\partial F/\partial h = T\partial(\ln Z)/\partial h$. This simply gives

$$M = h/\epsilon \ . \tag{1.22}$$

To find the zero-temperature spontaneous magnetization in the ordered phase, we need evaluate (1.22) for $T = 0$, $\alpha > \alpha_c$, and $h \to 0$. Using equations (1.20a) and (1.21a), we find

$$M = \sqrt{(\alpha - \alpha_c)/\alpha} \tag{1.23}$$

for the entire range $1 > s > 0$. The order parameter exponent β thus takes the value $1/2$ in the entire s-range. For $T > 0$, ϵ does not vanish even in the limit $h \to 0$. The spontaneous magnetization is therefore identical to zero for any nonzero temperature, independent of the dissipation strength α.

The critical magnetization-field curve of the quantum phase transition can be determined by analyzing (1.22) for $T = 0$, $\alpha = \alpha_c$, and nonzero h. In the case $1 > s > 1/2$, inserting (1.20b) into (1.22) yields

$$M = \left(A^s \alpha_c^{-1} \omega_c^{-(1-s)} h^{1-s}\right)^{1/(1+s)} \qquad (s > 1/2) \tag{1.24}$$

which implies a critical exponent $\delta = (1+s)/(1-s)$. For $s < 1/2$, we instead get the relation

$$M = \left(B \alpha_c^{-2} \omega_c^{-1} h\right)^{1/3} \qquad (s < 1/2) \ . \tag{1.25}$$

The critical exponent δ thus takes the mean-field value of 3.

4.2. SUSCEPTIBILITY. The Matsubara susceptibility can be calculated by taking the second derivative of $\ln Z$ in (1.11) with respect to the Fourier components of the field, yielding

$$\chi(i\omega_n) = \frac{1}{\epsilon + \alpha\omega_c^{1-s}|\omega_n|^s} \ . \tag{1.26}$$

We first discuss the static susceptibility $\chi_{\rm st} = \chi(0) = 1/\epsilon$ in the case $1 > s > 1/2$. To find the zero-temperature, zero-field susceptibility in the disordered (delocalized) phase, $\alpha < \alpha_c$, we use (1.14) for ϵ, which results in

$$\chi_{\rm st} = \alpha^{-1}\omega_c^{-1}A^{s/(1-s)}(\alpha_c - \alpha)^{-s/(1-s)} \quad (s > 1/2). \tag{1.27}$$

The susceptibility exponent thus takes the value $\gamma = s/(1-s)$.

For dissipation strengths $\alpha \geq \alpha_c$, the susceptibility diverges in the limit $T \to 0$. The temperature dependencies follow from substituting (1.17a) and (1.17b) into $\chi_{\rm st} = 1/\epsilon$. This yields

$$\chi_{\rm st} = \frac{\alpha - \alpha_c}{\alpha}\, T^{-1} \qquad (\alpha > \alpha_c,\ s > 1/2)\ , \tag{1.28a}$$

$$\chi_{\rm st} = \omega_c^{s-1}\alpha_c^{-1}A^s T^{-s} \quad (\alpha = \alpha_c,\ s > 1/2)\ . \tag{1.28b}$$

In the ordered (localized) phase, we thus find Curie behavior with an effective moment of $M^2 = (\alpha - \alpha_c)/\alpha$ in agreement with (1.23).

The static susceptibility in the case $s < 1/2$ is obtained analogously. Using (1.15), the zero-temperature, zero-field susceptibility reads

$$\chi_{\rm st} = \alpha^{-1}\omega_c^{-1}B(\alpha_c - \alpha)^{-1} \qquad (s < 1/2)\ , \tag{1.29}$$

implying that the susceptibility exponent takes the mean-field value $\gamma = 1$. From (1.18b), we obtain the temperature dependence of $\chi_{\rm st}$ at the critical damping strength,

$$\chi_{\rm st} = \omega_c^{-1}\alpha_c^{-1/2}B^{1/2}T^{-1/2} \quad (\alpha = \alpha_c,\ s < 1/2)\ . \tag{1.30}$$

In the ordered phase, the behavior for $s < 1/2$ is identical to that for $s > 1/2$ given in (1.28a).

We now turn to the dynamic susceptibility. To compute the retarded susceptibility $\chi(\omega)$, we need to analytically continue the Matsubara susceptibility by performing a Wick rotation to real frequencies, $i\omega_n \to \omega + i0$. A direct transformation of (1.26) is hampered by the non-analytic frequency dependence $|\omega_n|^s$. We therefore go back to a representation of the dynamic term in the susceptibility in terms of discrete bath modes [see the action (1.8)]. As this representation is analytic in ω_n, the Wick rotation can be performed easily. We then carry out the integration over the spectral density *after* the Wick rotation. The resulting dynamical susceptibility reads

$$\chi(\omega) = \frac{1}{\epsilon + \alpha\omega_c^{1-s}|\omega|^s\left[\cos(\pi s/2) - i\sin(\pi s/2)\mathrm{sgn}(\omega)\right]}\ . \tag{1.31}$$

At quantum criticality ($\alpha = \alpha_c$, $T = 0$, $h = 0$), the real and imaginary parts of the dynamic susceptibility simplify to

$$\mathrm{Re}\chi(\omega) = \frac{\cos(\pi s/2)}{\alpha_c\omega_c^{1-s}|\omega|^s}\ ,\ \ \mathrm{Im}\chi(\omega) = \frac{\sin(\pi s/2)\mathrm{sgn}(\omega)}{\alpha_c\omega_c^{1-s}|\omega|^s} \tag{1.32}$$

in the entire range $1 > s > 0$. Comparing this with the temperature dependencies (1.28b) and (1.30), we note that the results for $s < 1/2$ violate ω/T scaling while those for $1 > s > 1/2$ are compatible with it.

4.3. CORRELATION TIME. To find the inverse correlation time (characteristic energy) $\Delta = \xi_t^{-1}$, we parameterize the inverse susceptibility as $\epsilon + \alpha\omega_c^{1-s}|\omega_n|^s =$

$\epsilon(1 + |\omega_n/\Delta|^s)$. This implies the relation

$$\Delta = \left(\epsilon\alpha^{-1}\omega_c^{s-1}\right)^{1/s} \ . \tag{1.33}$$

The dependence of the inverse correlation time on the tuning parameter α at zero temperature and field in the case $1 > s > 1/2$ is obtained by inserting (1.14) into (1.33). In the disordered phase, $\alpha < \alpha_c$, this gives

$$\Delta = \omega_c A^{-1/(1-s)}(\alpha_c - \alpha)^{1/(1-s)} \qquad (s > 1/2) \ . \tag{1.34}$$

The correlation-time critical exponent therefore reads $\nu z = 1/(1-s)$. Note that this exponent is sometimes called just ν rather than νz in the literature on impurity transitions. We follow the general convention for quantum phase transitions where ν describes the divergence of the correlation *length* while νz that of the correlation *time*. By substituting (1.17b) into (1.33), we can also determine the dependence of Δ on temperature at $\alpha = \alpha_c$ and $h = 0$. We find $\Delta = A^{-1}T$. The characteristic energy thus scales with T, as expected from naive scaling.

In the case $s < 1/2$, the zero-temperature, zero-field correlation time in the disordered phase behaves as [using (1.15)]

$$\Delta = \omega_c B^{-1/s}(\alpha_c - \alpha)^{1/s} \qquad (s < 1/2) \ , \tag{1.35}$$

resulting in the mean-field value $\nu z = 1/s$ for the correlation time critical exponent. The dependence of Δ on temperature at $\alpha = \alpha_c$ and $h = 0$ follows from (1.18b); it reads $\Delta = B^{-1/(2s)}\omega_c^{(2s-1)/(2s)}T^{1/(2s)}$. The characteristic energy thus scales differently than the temperature, in disagreement with naive scaling.

4.4. SCALING FORM OF THE EQUATION OF STATE. A scaling form of the equation of state for $1 > s > 1/2$ can be determined by subtracting the quantum critical ($T = 0$, $h = 0$, $\alpha = \alpha_c$) spherical constraint from the general

constraint (1.12). After performing the resulting integral, we find

$$\frac{\alpha_c - \alpha}{\alpha} + \frac{h^2}{\epsilon^2} + \frac{T}{\epsilon} = A\epsilon^{-1+1/s}\alpha^{-1/s}\omega_c^{1-1/s} \ . \tag{1.36}$$

We substitute $\epsilon = h/M$ [from (1.22)]; and after some lengthy but straight forward algebra, this equation can be written in the scaling form

$$X\left(M/r^{1/2}, h/r^{(1+s)/(2-2s)}, T/r^{1/(1-s)}\right) = 0, \tag{1.37}$$

with X being the scaling function, and $r = (\alpha - \alpha_c)/\alpha$ being the reduced distance from criticality. This scaling form can be used to reproduce the critical exponents $\beta = 1/2$, $\gamma = s/(1-s)$, and $\delta = (1+s)/(1-s)$ found above.

For $s < 1/2$, the same approach gives a scaling equation containing the mean-field exponents $\beta = 1/2$, $\gamma = 1$, and $\delta = 3$. Moreover, an explicit dependence on the cutoff for the Matsubara frequencies remains.

4.5. ENTROPY AND SPECIFIC HEAT. Within our path integral approach, thermal properties are somewhat harder to calculate than magnetic properties because the measure of the path integral explicitly depends on temperature. As the spherical model is equivalent to a set of coupled harmonic oscillators, we can use the "remarkable formulas" derived by Ford et al., [80, 81] which express the free energy (and internal energy) of a quantum oscillator in a heat bath in terms of its susceptibility and the free energy (and internal energy) of a free oscillator. For our spherical model, they read

$$F_S = -\mu + \frac{1}{\pi}\int_0^\infty d\omega\, F_f(\omega, T)\, \mathrm{Im}\left[\frac{d}{d\omega}\ln\chi(\omega)\right] \ , \tag{1.38}$$

$$U_S = -\mu + \frac{1}{\pi}\int_0^\infty d\omega\, U_f(\omega, T)\, \mathrm{Im}\left[\frac{d}{d\omega}\ln\chi(\omega)\right] \ . \tag{1.39}$$

Here, $F_f(\omega, T) = T\ln[2\sinh(\omega/2T)]$ and $U_f(\omega, T) = (\omega/2)\coth(\omega/2T)$. The extra $-\mu$ terms stem from the spherical constraint. Note that the free energy in (1.38) is

the difference between the free energy of the coupled rotor-bath system and that of the unperturbed bath, $F_S = F - F_B^0 = -T \ln(Z/Z_B^0)$. The same holds true for the internal energy, $U_S = U - U_B^0$.

The frequency derivative of $\ln \chi(\omega)$ can be calculated from (1.31), giving

$$\begin{aligned} &\mathrm{Im}\left[\frac{d}{d\omega} \ln \chi(\omega)\right] = \\ &= \frac{\epsilon s \alpha \omega_c^{1-s} \omega^{s-1} \sin(\pi s/2)}{[\epsilon + \alpha \omega_c^{1-s} \omega^s \cos(\pi s/2)]^2 + [\alpha \omega_c^{1-s} \omega^s \sin(\pi s/2)]^2}. \end{aligned} \tag{1.40}$$

To calculate the impurity entropy $S_S = (U_S - F_S)/T$, we insert (1.40) into (1.38) and (1.39) and perform the resulting integral. In the disordered phase, $\alpha < \alpha_c$, the entropy behaves as

$$S_S = D\, \alpha\, \omega_c^{1-s} T^s / \epsilon_0 \tag{1.41}$$

in the limit $T \to 0$ for all s in the sub-Ohmic range $1 > s > 0$. Here, ϵ_0 is the zero-temperature renormalized distance from criticality given in (1.14), and D is an s-dependent constant. Upon approaching criticality, $\alpha \to \alpha_c$, the prefactor of the T^s power-law diverges, suggesting a weaker temperature dependence at criticality. The specific heat can be calculated from $C_S = T(\partial S_S/\partial T)$, it thus behaves as $Ds\alpha\omega_c^{1-s}T^s/\epsilon_0$.

We now turn to the critical dissipation strength, $\alpha = \alpha_c$, For $1 > s > 1/2$, we find a temperature-independent but non-universal (s-dependent) entropy in the limit of low temperatures. For $s < 1/2$, the impurity entropy diverges logarithmically as $\ln(\omega_0/T)$ with $T \to 0$. In the ordered phase, $\alpha > \alpha_c$, we find a logarithmically diverging entropy for all s between 0 and 1.

At first glance, these logarithmic divergencies appear to violate the third law of thermodynamics. We emphasize, however, that the impurity entropy represents the difference between the entropy of the coupled rotor-bath system and that of the unperturbed bath. Because the bath is infinite, the entropy thus involves an *infinite*

number of degrees of freedom and does not have to remain finite. Whether the logarithmic divergence occurs only in the large-N limit or also for finite-N rotors remains a question for the future.

We note in passing that the entropy of classical spherical models [76, 82] also diverges in the limit $T \to 0$ (even when measured per degree of freedom). In these models, the diverges occurs because the classical description becomes invalid at sufficiently low temperatures. It can be cured by going from the classical spherical model to the quantum spherical model [77]. This implies that the diverging entropy in the ordered phase of the sub-Ohmic rotor model is caused by a different mechanism than that in the classical spherical model.

5. CONCLUSIONS

In summary, we have investigated the quantum critical behavior of a large-N quantum rotor coupled to a sub-Ohmic bosonic bath characterized by a power-law spectral density $J(\omega) \sim \omega^s$ with $0 < s < 1$. As this model can be solved exactly, it provides a reliable reference point for the discussion of more complex and realistic impurity quantum phase transitions. We find that all critical exponents take their mean-field values if the bath exponent s is below $1/2$. In contrast, for $1 > s > 1/2$, the exponents display nontrivial, s-dependent values. A summary of the exponent values in both cases in shown in table 5.1. The exponent η sticks to its mean-field value $2-s$ in the entire region $1 > s > 0$, in agreement with renormalization group arguments on the absence of field renormalization for long-range interactions [83, 84, 85]. The fact that the order parameter exponent β is $1/2$ in the entire range $1 > s > 0$ is a results of the large-N limit; it generically takes this value in spherical models.

Moreover, the behaviors of the dynamic susceptibility and inverse correlation time are compatible with ω/T scaling for $1 > s > 1/2$, while they violate ω/T scaling for $s < 1/2$. We conclude that the quantum phase transition of the sub-Ohmic quantum rotor model is controlled by an interacting renormalization group fixed point in the case $1 > s > 1/2$. In contrast, the transition is controlled by a noninteracting (Gaussian) fixed point for $s < 1/2$.

Table 5.1: Critical exponents of the sub-Ohmic quantum rotor model.

	$1 > s > 1/2$	$s < 1/2$
β	$1/2$	$1/2$
γ	$s/(1-s)$	1
δ	$(1+s)/(1-s)$	3
νz	$1/(1-s)$	$1/s$
η	$2-s$	$2-s$

We now turn to the question of the quantum-to-classical mapping. The classical counterpart of the sub-Ohmic quantum rotor model is a one-dimensional classical Heisenberg chain with long-range interactions that decay as $1/r^{1+s}$ with distance r. The spherical (large-N) version of this model was solved by Joyce; [76] its critical exponents are identical to that of the sub-Ohmic quantum rotor found here. The quantum-to-classical mapping is thus valid.

The properties of our quantum *rotor* model must be contrasted with the behavior of the Bose-Kondo model which describes a continuous symmetry quantum *spin* coupled to a bosonic bath. For this system, the quantum-to-classical mapping appears to be inapplicable [72]. A related observation has been made in a Bose-Fermi-Kondo model [73]. The main difference between a rotor and a quantum spin is the presence of the Berry phase term in the action of the latter. Our results thus support the conjecture that this Berry phase term, which is complex and has no classical analog, causes the inapplicability of the quantum-to-classical mapping.

6. ACKNOWLEDGEMENTS

We acknowledge helpful discussions with M. Vojta and S. Kirchner. This work has been supported in part by the NSF under grant no. DMR-0906566.

II. PERCOLATION TRANSITION IN QUANTUM ISING AND ROTOR MODELS WITH SUB-OHMIC DISSIPATION

Manal Al-Ali[1], José A Hoyos[2], and Thomas Vojta[1]

[1]Department of Physics, Missouri University of Science and Technology, Rolla, MO 65409, USA

[2]Instituto de Física de São Carlos, Universidade de São Paulo, C.P. 369, São Carlos, São Paulo 13560-970, Brazil

[1]*Department of Physics, Missouri University of Science & Technology, Rolla, MO 65409*

ABSTRACT*

We investigate the influence of sub-Ohmic dissipation on randomly diluted quantum Ising and rotor models. The dissipation causes the quantum dynamics of sufficiently large percolation clusters to freeze completely. As a result, the zero-temperature quantum phase transition across the lattice percolation threshold separates an unusual super-paramagnetic cluster phase from an inhomogeneous ferromagnetic phase. We determine the low-temperature thermodynamic behavior in both phases which is dominated by large frozen and slowly fluctuating percolation clusters. We relate our results to the smeared transition scenario for disordered quantum phase transitions, and we compare the cases of sub-Ohmic, Ohmic, and super-Ohmic dissipation.

*Published in Physical Review B 86, 075119 (2012)

1. INTRODUCTION

The interplay between geometric, quantum, and thermal fluctuations in randomly diluted quantum many-particle systems leads to a host of unconventional low-temperature phenomena. These include the singular thermodynamic and transport properties in quantum Griffiths phases [86, 87] as well as the exotic scaling behavior of the quantum phase transitions between different ground state phases [39, 40]. Recent reviews of this topic can be found, e.g., in Refs. [30, 31].

An especially interesting situation arises if a quantum many-particle system is diluted beyond the percolation threshold p_c of the underlying lattice (see, e.g., Ref. [88] and references therein). Although the resulting percolation quantum phase transition is driven by the geometric fluctuations of the lattice, the quantum fluctuations lead to critical behavior different from that of classical percolation. In the case of a diluted transverse-field Ising magnet, the transition displays exotic activated (exponential) dynamic scaling [89] similar to what is observed at infinite-randomness critical points [39, 40]. The percolation transition of the quantum rotor model shows conventional scaling (at least in the particle-hole symmetric case where topological Berry phase terms are unimportant [90]), but with critical exponents that differ from their classical counterparts [91, 92]. For site-diluted Heisenberg quantum antiferromagnets, further modifications of the critical behavior were attributed to uncompensated geometric Berry phases [93, 94].

In many realistic systems, the relevant degrees of freedom are coupled to an environment of "heat-bath" modes. The resulting dissipation can qualitatively change the low-energy properties of a quantum many-particle system. In particular, it has been shown that dissipation can further enhance the effects of randomness on quantum phase transitions. In generic random quantum Ising models, for instance, the presence of Ohmic dissipation completely destroys the sharp quantum phase transition by smearing [46, 47, 95, 96, 97, 98]. while it leads to infinite-randomness critical behavior

in systems with continuous-symmetry order parameter [99, 100, 101]. Interestingly, super-Ohmic dissipation does not change the universality class of random quantum Ising models [97, 98] but plays a major role in systems with continuous-symmetry order parameter [102].

It is therefore interesting to ask what are the effects of dissipation on randomly diluted quantum many-particle systems close to the percolation threshold. It has recently been shown that Ohmic dissipation in a diluted quantum Ising model leads to an unusual percolation quantum phase transition [103] at which some observables show classical critical behavior while others are modified by quantum fluctuations.

In the present paper, we focus on the influence of sub-Ohmic dissipation (which is qualitatively stronger than the more common Ohmic dissipation) on diluted quantum Ising models and quantum rotor models. When coupled to a sub-Ohmic bath, even a single quantum spin displays a nontrivial quantum phase transition from a fluctuating to a localized phase [29] whose properties have attracted considerable attention recently (see, e.g., Ref. [64] and references therein). Accordingly, we find that the quantum dynamics of sufficiently large percolation clusters freezes completely as a result of the coupling to the sub-Ohmic bath, effectively turning them into classical moments. The interplay between large frozen clusters and smaller dynamic clusters gives rise to unconventional properties of the percolation transition which we explore in detail.

Our paper is organized as follows: In Sec. 2., we define our models and discuss their phase diagrams at a qualitative level. Section 3. is devoted to a detailed analysis of the quantum rotor model in the large-N limit where all calculations can be performed explicitly. In Sec. 4., we go beyond the large-N limit and develop a general scaling approach. We conclude in Sec. 4..

2. MODELS AND PHASE DIAGRAMS

2.1. DILUTED DISSIPATIVE QUANTUM ISING AND ROTOR MODELS.

We consider two models. The first model is a d-dimensional ($d \geq 2$) site-diluted transverse-field Ising model [54, 55, 56, 57] given by the Hamiltonian

$$H_I = -J \sum_{\langle i,j \rangle} \eta_i \eta_j \sigma_i^z \sigma_j^z - h_x \sum_i \eta_i \sigma_i^x \ , \tag{2.1}$$

a prototypical disordered quantum magnet. The Pauli matrices σ_i^z and σ_i^x represent the spin components at site i, the exchange interaction J couples nearest neighbor sites, and the transverse field h_x controls the quantum fluctuations. Dilution is introduced via the random variables η_i which can take the values 0 and 1 with probabilities p and $1-p$, respectively. We now couple each spin to a local heat bath of harmonic oscillators [96, 104],

$$H = H_I + \sum_{i,n} \eta_i \left[\nu_{i,n} a_{i,n}^\dagger a_{i,n} + \frac{1}{2} \lambda_{i,n} \sigma_i^z (a_{i,n}^\dagger + a_{i,n}) \right], \tag{2.2}$$

where $a_{i,n}$ ($a_{i,n}^\dagger$) is the annihilation (creation) operator of the n-th oscillator coupled to spin i; $\nu_{i,n}$ is its natural frequency, and $\lambda_{i,n}$ is the coupling constant. All baths have the same spectral function

$$\mathcal{E}(\omega) = \pi \sum_n \lambda_{i,n}^2 \delta(\omega - \nu_{i,n}) = 2\pi\alpha\omega_c^{1-\zeta}\omega^\zeta e^{-\omega/\omega_c}, \tag{2.3}$$

with α and ω_c being the dimensionless dissipation strength and the cutoff energy, respectively. The exponent ζ characterizes the type of dissipation; we are mostly interested in the sub-Ohmic case $0 < \zeta < 1$. For comparison, we will also consider the Ohmic ($\zeta = 1$) and super-Ohmic cases ($\zeta > 1$). Experimentally, local dissipation (with various spectral densities) can be realized, e.g., in molecular magnets weakly

coupled to nuclear spins [105, 106] or in magnetic nanoparticles in an insulating host [107].

The second model is a site-diluted dissipative quantum rotor model which can be conveniently defined in terms of the effective Euclidean (imaginary time) action [91]

$$\begin{aligned} \mathcal{A} &= \int \mathrm{d}\tau \sum_{\langle ij \rangle} J \eta_i \eta_j \boldsymbol{\phi}_i(\tau) \cdot \boldsymbol{\phi}_j(\tau) + \sum_i \eta_i \mathcal{A}_{\mathrm{dyn}}[\boldsymbol{\phi}_i] \\ \mathcal{A}_{\mathrm{dyn}}[\boldsymbol{\phi}] &= \frac{\alpha}{2} T \sum_{\omega_n} \omega_c^{1-\zeta} |\omega_n|^{\zeta} \; \tilde{\boldsymbol{\phi}}(\omega_n) \cdot \tilde{\boldsymbol{\phi}}(-\omega_n) \; . \end{aligned} \tag{2.4}$$

Here, the random variables $\eta_i = 0, 1$ again implement the site dilution, and ω_n are bosonic Matsubara frequencies. The rotor at site i and imaginary time τ is described by $\boldsymbol{\phi}_i(\tau)$: a N-component vector of length $N^{1/2}$. Its Fourier transform in imaginary time is denoted by $\tilde{\boldsymbol{\phi}}(\omega_n)$. The dynamic action $\mathcal{A}_{\mathrm{dyn}}$ stems from integrating out the heat-bath modes, with the parameter α measuring the strength of the dissipation, and the exponent ζ characterizing the type of the dissipation, as in the first model [see Eq. (2.3)].

2.2. CLASSICAL PERCOLATION THEORY. We now briefly summarize the results of percolation theory [53] to the extent necessary for our purposes.

Consider a regular d-dimensional lattice in which each site is removed at random with probability p.[†] For small p, the resulting diluted lattice is still connected in the sense that there is a cluster of connected nearest neighbor sites (called the percolating cluster) that spans the entire system. For large p, on the other hand, a percolating cluster does not exist. Instead, the lattice is made up of many isolated clusters consisting of just a few sites.

In the thermodynamic limit of infinite system volume, the two regimes are separated by a sharp geometric phase transition at the percolation threshold $p = p_c$. The behavior of the lattice close to p_c can be understood as a geometric critical

[†]In agreement with Subsec. 2.1, we define p as the fraction of sites removed rather than the fraction of sites present.

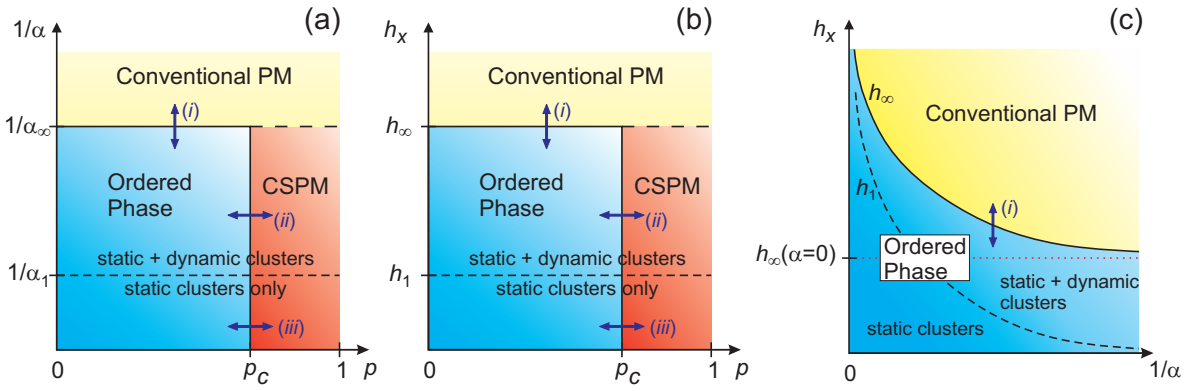

Figure 2.1: (Color online) Schematic ground state phase diagram of the diluted dissipative quantum Ising model Eq. (2.2) for fixed values of $\zeta < 1$, ω_c, and J. The three panels show three cuts through the three-dimensional parameter space of dilution p, transverse field h_x, and dissipation strength α. (a) α–p phase diagram at a fixed transverse field h_x with $h_x > h_\infty(\alpha = 0)$ such that the dissipationless system is in the paramagnetic phase. This phase diagram also applies to the rotor model Eq. (2.4). (b) h_x–p phase diagram at a fixed dissipation strength α. (c) h_x–α phase diagram at fixed dilution $p < p_c$. CSPM refers to the cluster super-paramagnetic phase, transition (i) denotes the smeared generic (field or dissipation-driven) quantum phase transition, and (ii) and (iii) denote the percolation quantum phase transitions in the two regimes with or without dynamic clusters, respectively.

phenomenon. The order parameter is the probability P_∞ of a site to belong to the infinite connected percolation cluster. It is obviously zero in the disconnected phase ($p > p_c$) and nonzero in the percolating phase ($p < p_c$). Close to p_c, it varies as

$$P_\infty \sim |p - p_c|^{\beta_c} \qquad (p < p_c) \tag{2.5}$$

where β_c is the order parameter critical exponent of classical percolation. (We use a subscript c to distinguish quantities associated with the lattice percolation transition from those of the quantum phase transitions discussed below). In addition to the infinite cluster, we also need to characterize the finite clusters on both sides of the percolation threshold. Their typical size, the correlation or connectedness length ξ_c,

diverges as

$$\xi_c \sim |p - p_c|^{-\nu_c} \tag{2.6}$$

with ν_c the correlation length exponent. The average mass S_c (number of sites) of a finite cluster diverges with the susceptibility exponent γ_c according to

$$S_c \sim |p - p_c|^{-\gamma_c} \ . \tag{2.7}$$

The complete information about the percolation critical behavior is contained in the cluster size distribution n_s, i.e., the number of clusters with s sites excluding the infinite cluster (normalized by the total number of lattice sites). Close to the percolation threshold, it obeys the scaling form

$$n_s(p) = s^{-\tau_c} f\left[(p - p_c)s^{\sigma_c}\right]. \tag{2.8}$$

Here, τ_c and σ_c are critical exponents. The scaling function $f(x)$ is analytic for small x and has a single maximum at some $x_{\max} > 0$. For large $|x|$, it drops off rapidly

$$f(x) \sim \exp\left(-B_1 x^{1/\sigma_c}\right) \qquad (x > 0), \tag{2.9}$$

$$f(x) \sim \exp\left[-\left(B_2 x^{1/\sigma_c}\right)^{1-1/d}\right] \qquad (x < 0), \tag{2.10}$$

where B_1 and B_2 are constants of order unity. The classical percolation exponents are determined by τ_c and σ_c: the correlation lengths exponent $\nu_c = (\tau_c - 1)/(d\sigma_c)$, the order parameter exponent $\beta_c = (\tau_c - 2)/\sigma_c$, and the susceptibility exponent $\gamma_c = (3 - \tau_c)/\sigma_c$.

Right at the percolation threshold, the cluster size distribution does not contain a characteristic scale, $n_s \sim s^{-\tau_c}$, yielding a fractal critical percolation cluster of fractal dimension $D_f = d/(\tau_c - 1)$.

2.3. PHASE DIAGRAMS. Let us now discuss in a qualitative fashion the phase diagrams of the models introduced in Subsec. 2.1, beginning with the diluted dissipative quantum Ising model Eq. (2.2). If we fix the bath parameters ζ and ω_c and measure all energies in terms of the exchange interaction J, we still need to explore the phases in the three-dimensional parameter space of transverse field h_x, dissipation strength α and dilution p. A sketch of the phase diagram is shown in Fig. 2.1. For sufficiently large transverse field and/or sufficiently weak dissipation, the ground state is paramagnetic for all values of the dilution p. This is the conventional paramagnetic phase that can be found for $h_x > h_\infty(\alpha)$ or, correspondingly, for $\alpha < \alpha_\infty(h_x)$. Here, $h_\infty(\alpha)$ is the transverse field at which the undiluted bulk system undergoes the transition at fixed α while $\alpha_\infty(h_x)$ is its critical dissipation strength at fixed h_x.

The behavior for $h_x < h_\infty(\alpha)$ [or $\alpha > \alpha_\infty(h_x)$] depends on the dilution p. It is clear that magnetic long-range order is impossible for $p > p_c$, because the lattice consists of finite-size clusters that are completely decoupled from each other. Each of these clusters acts as an independent magnetic moment. For $h_x < h_\infty(\alpha)$ and $p > p_c$, the system is thus in a cluster super-paramagnetic phase.

Let us consider a single cluster of s sites in more detail. For small transverse fields, its low-energy physics is equivalent to that of a sub-Ohmic spin-boson model, i.e., a single effective Ising spin (whose moment is proportional to s) in an effective transverse-field $h_x(s) \sim h_x e^{-Bs}$ with $B \sim \ln(J/h_x)$ and coupled to a sub-Ohmic bath with an effective dissipation strength $\alpha_s = s\alpha$ [89, 103]. With increasing dissipation strength and/or decreasing transverse field, this sub-Ohmic spin-boson model undergoes a quantum phase transition from a fluctuating to a localized (frozen) ground state [29]. This implies that sufficiently large percolation clusters are in the localized phase, i.e., they behave as classical moments. The cluster super-paramagnetic phase thus consists of two regimes. If the transverse field is not too small, $h_1(\alpha) < h_x < h_\infty(\alpha)$ [or if the dissipation is not too strong,

$\alpha_1(h_x) > \alpha > \alpha_\infty(h_x)$], static and dynamic clusters coexist. Here, $h_1(\alpha)$ is the critical field of a *single* spin in a bath of dissipation strength α while $\alpha_1(h_x)$ is its critical dissipation strength in a given field h_x. In contrast, for $h_x < h_1(\alpha)$ [or $\alpha > \alpha_1(h_x)$], all clusters are frozen, and the system behaves purely classically.

Finally, for dilutions $p < p_c$, there is an infinite-spanning percolation cluster that can support magnetic long-range order. Naively, one might expect that the critical transverse-field (at fixed dissipation strength α) decreases with dilution p because the spins are missing neighbors. However, in our case of sub-Ohmic dissipation, rare vacancy-free spatial regions can undergo the quantum phase transition independently from the bulk system. As a consequence, the field-driven transition [transition (i) in Fig. 2.1] is smeared, [46, 47] and the ordered phase extends all the way to the clean critical field $h_\infty(\alpha)$ for all $p < p_c$. Analogous arguments apply to the critical dissipation strength at fixed transverse field h_x.

The infinite percolation cluster coexists with a spectrum of isolated finite-size clusters whose behavior depends on the transverse field and dissipation strength. Analogous to the super-paramagnetic phase discussed above, the ordered phase thus consists of two regimes. For $h_1(\alpha) < h_x < h_\infty(\alpha)$ [or $\alpha_1(h_x) > \alpha > \alpha_\infty(h_x)$], static (frozen) and dynamic clusters coexist with the long-range-ordered infinite cluster. For $h_x < h_1(\alpha)$ [or $\alpha > \alpha_1(h_x)$], all clusters are frozen, and the system behaves classically.

The phase diagram of the diluted quantum rotor model with sub-Ohmic dissipation (2.4) can be discussed along the same lines. After fixing the bath parameters ζ and ω_c and measuring all energies in terms of the exchange interaction J, we are left with two parameters, the dilution p and the dissipation strength α. The zero-temperature behavior of a single quantum rotor coupled to a sub-Ohmic bath is analogous to that of the corresponding quantum Ising spin. With increasing dissipation strength, the rotor undergoes a quantum phase transition from a fluctuating to a localized ground state. This follows, for instance, from mapping [3] the sub-Ohmic quantum rotor model onto a one-dimensional classical Heisenberg chain with

an interaction that falls off more slowly than $1/r^2$. This model is known to have an ordered phase for sufficiently strong interactions [108]. As a result, all the arguments used above to discuss the phase diagram of the diluted sub-Ohmic transverse-field Ising model carry over to the rotor model Eq. (2.4). The α–p phase diagram of the rotor model thus agrees with the phase diagram shown in Fig. 2.1(a).

In the following sections, we investigate the percolation quantum phase transitions of the models Eqs. (2.2) and (2.4), i.e., the transitions occurring when the dilution p is tuned through the lattice percolation threshold p_c. These transitions are marked in Fig. 2.1 by (ii) and (iii).

3. DILUTED QUANTUM ROTOR MODEL IN THE LARGE-N LIMIT

In this section, we focus on the diluted dissipative quantum rotor model in the large-N limit of an infinite number of order-parameter components. In this limit, the problem turns into a self-consistent Gaussian model. Consequently, all calculations can be performed explicitly.

3.1. SINGLE PERCOLATION CLUSTER. We begin by considering a single percolation cluster of s sites. For $\alpha > \alpha_\infty$, this cluster is locally in the ordered phase. Following Refs. [109, 110], it can therefore be described as a single large-N rotor with moment s coupled to a sub-Ohmic dissipative bath of strength $\alpha_s = s\alpha$. Its effective action is given by

$$\mathcal{A}_{\text{eff}} = T\sum_{\omega_n}\left[\frac{1}{2}\tilde{\psi}(\omega_n)\Gamma_n\tilde{\psi}(-\omega_n) - s\tilde{H}_z(\omega_n)\tilde{\psi}(-\omega_n)\right] \tag{2.11}$$

where $\Gamma_n = \epsilon + s\alpha\omega_c^{1-\zeta}|\omega_n|^\zeta$, ψ represents one rotor component and H_z is an external field conjugate to the order parameter.

In the large-N limit, the renormalized distance ϵ from criticality of the cluster is fixed by the large-N (spherical) constraint $\langle|\psi(\tau)|^2\rangle = 1$. In terms of the Fourier transform, $\tilde{\psi}(\omega_n)$ defined by

$$\psi(\tau) = T\sum_{\omega_n}\tilde{\psi}(\omega_n)\exp\left[-i\omega_n\tau\right], \tag{2.12}$$

the large-N constraint for a constant field H_z becomes

$$T\sum_{\omega_n}\frac{1}{\epsilon + s\alpha\omega_c^{1-\zeta}|\omega_n|^\zeta} + \left(\frac{sH_z}{\epsilon}\right)^2 = 1. \tag{2.13}$$

Solving this equation gives the renormalized distance from criticality ϵ as a function of the cluster size s.

At zero temperature and field, the sum over the Matsubara frequencies turns into an integration, and the constraint equation reads

$$\frac{1}{\pi}\int_0^{\omega_c} \mathrm{d}\omega \frac{1}{\epsilon_0 + s\alpha\omega_c^{1-\zeta}|\omega|^\zeta} = 1. \tag{2.14}$$

(We denote the renormalized distance from criticality at zero temperature and field by ϵ_0.) The critical size s_c above which the cluster freezes can be found by setting $\epsilon_0 = 0$ and performing the integral (2.14). This gives

$$s_c = 1/\left[\pi\alpha(1-\zeta)\right]. \tag{2.15}$$

As we are interested in the critical behavior of the clusters, we now solve the constraint equation for cluster sizes close to the critical one, $s_c - s \ll s_c$. This can be accomplished by subtracting the constraints at s and s_c from each other. We need to distinguish two cases: $1/2 < \zeta < 1$ and $\zeta < 1/2$. In the first case, the resulting integral can be easily evaluated after moving the cut-off ω_c to infinity. This gives

$$\epsilon_0 = \alpha s_c[-\zeta\sin(\pi/\zeta)\alpha(s_c - s)]^{\zeta/(1-\zeta)}\omega_c \quad (\text{for } \zeta > 1/2). \tag{2.16}$$

In the second case, $\zeta < 1/2$, we can evaluate Eq. (2.14) via a straight Taylor expansion in $(s_c - s)$. This results in

$$\epsilon_0 = \alpha^2 s_c \pi(1-2\zeta)(s_c - s)\omega_c \quad (\text{for } \zeta < 1/2). \tag{2.17}$$

It will be useful to rewrite Eqs. (2.16) and (2.17) in a more compact manner:

$$\epsilon_0(s) = [A_\zeta(1 - s/s_c)]^{x/(1-x)}\omega_c, \tag{2.18}$$

where $A_\zeta = -(\alpha s_c)^{1/\zeta}\zeta\sin(\pi/\zeta)$ for $\zeta > 1/2$, and $A_\zeta = (\alpha s_c)^2\pi(1-2\zeta)$ for $\zeta < 1/2$, and $x = \max\{1/2, \zeta\}$.

In order to compute thermodynamic quantities, we will also need the value of $\epsilon(s)$ at non zero temperature. The constraint equation for small but nonzero temperature can be obtained by keeping the $\omega_n = 0$ term in the frequency sum of Eq. (2.13) discrete, while representing all other modes in terms of an ω-integral. This gives

$$\frac{T}{\epsilon} + \frac{1}{\pi}\int_0^{\omega_c} \mathrm{d}\omega \frac{1}{\epsilon + s\alpha\omega_c^{1-\zeta}|\omega|^\zeta} = 1. \tag{2.19}$$

Solving this equation for asymptotically low temperatures results in the following behaviors. For clusters larger than the critical size, $s > s_c$, ϵ vanishes linearly with T via $\epsilon = Ts/(s - s_c)$. Clusters of exactly the critical size have $\epsilon = A_\zeta^x \omega_c^{1-x} T^x$. For smaller clusters ($s < s_c$), low temperatures only lead to a small correction of the zero-temperature behavior ϵ_0. Writing $\epsilon(T) = \epsilon_0 + \delta T$, we obtain $\delta = [s/(s_c - s)][x/(1 - x)]$. Clusters with sizes close to the critical one show a crossover from the off-critical to the critical regime with increasing T. For $s \lesssim s_c$, this means

$$\epsilon(T) \approx \begin{cases} \epsilon_0(1 + \delta T/\epsilon_0) & (\text{for } \epsilon_0 \gg \epsilon_T), \\ \epsilon_T & (\text{otherwise}), \end{cases} \tag{2.20}$$

with $\epsilon_T = A_\zeta^x \omega_c^{1-x} T^x$.

The constraint equation at zero temperature but in a nonzero ordering field H_z can be solved analogously [110]. For asymptotically small fields, we find $\epsilon(H_z) = sH_z[s/(s - s_c)]^{1/2}$ in the case of clusters of size $s > s_c$. At the critical size, $\epsilon(H_z) = [A_\zeta^x \omega_c^{1-x}(s_c H_z)^{2x}]^{1/(1+x)}$, and for $s < s_c$ we obtain $\epsilon(H_z) = \epsilon_0 + \delta(sH_z)^2/\epsilon_0$. Larger fields lead to a crossover from the off-critical to the critical regime. For $s \lesssim s_c$, it reads

$$\epsilon(H_z) \approx \begin{cases} \epsilon_0[1 + \delta(sH_z/\epsilon_0)^2] & (\text{for } \epsilon_0 \gg \epsilon_{H_z}), \\ \epsilon_{H_z} & (\text{otherwise}), \end{cases} \tag{2.21}$$

with $\epsilon_{H_z} = [A_\zeta^x \omega_c^{1-x}(sH_z)^{2x}]^{1/(1+x)}$.

Observables of a single cluster can now be determined by taking the appropriate derivatives of the free energy $F_{cl} = -T\ln(Z)$ with

$$Z = \prod_n Z_n \tag{2.22}$$

where

$$Z_n = \frac{T}{\epsilon + s\alpha\omega_c^{1-\zeta}|\omega_n|^\zeta} \exp\left(\frac{T}{2}\frac{s\tilde{H}_z(\omega_n)s\tilde{H}_z(-\omega_n)}{\epsilon + s\alpha\omega_c^{1-\zeta}|\omega_n|^\zeta}\right). \tag{2.23}$$

The dynamical (Matsubara) susceptibility and magnetization are then given by

$$\chi_{cl}(i\omega_n) = \frac{s^2}{\epsilon + s\alpha\omega_c^{1-\zeta}|\omega_n|^\zeta}\ , \tag{2.24}$$

and

$$m_{cl}(\omega_n) = T\frac{s^2\tilde{H}_z(\omega_n)}{\epsilon + s\alpha\omega_c^{1-\zeta}|\omega_n|^\zeta}\ , \tag{2.25}$$

respectively, where ϵ is given by the solution of constraint equation discussed above. (Note that the contribution of a cluster of size s to the uniform susceptibility is proportional to s^2). Therefore, in the above two limiting cases, we can write the uniform and static susceptibility of a cluster of size $s < s_c$ as a function of temperature as follows

$$\chi_{cl}(T) \approx s^2/\epsilon(T). \tag{2.26}$$

Large clusters ($s > s_c$) behave classically, $\chi_{cl} \approx s(s - s_c)/T$, at low-temperatures. Finally, for the critical ones $\chi_{cl} \approx s^2/\epsilon_T$.

In order to calculate the retarded susceptibility $\chi_{cl}(\omega)$, we need to analytically continue the Matsubara susceptibility by performing a Wick rotation to real frequency, $i\omega_n \to \omega + i0$. The resulting dynamical susceptibility reads

$$\chi_{cl}(\omega) = \frac{s^2}{\epsilon + \alpha\omega_c^{1-\zeta}|\omega|^\zeta\left[\cos(\pi\zeta/2) - i\sin(\pi\zeta/2)\mathrm{sgn}(\omega)\right]}. \tag{2.27}$$

Using Eq. (2.21), the single cluster magnetization in a small ordering constant field H_z is given by

$$m_{cl} = \chi_{cl} H_z \approx \begin{cases} H_z s^2/\epsilon_0 & (\text{for } \epsilon_0 \gg \epsilon_{H_z}), \\ H_z s^2/\epsilon_{H_z} & (\text{otherwise}). \end{cases} \tag{2.28}$$

Thermal properties (at zero field) can be computed by using the "remarkable formulas" derived by Ford *et al.*, [81] which express the free energy (the internal energy) of a quantum oscillator in a heat bath in terms of its susceptibility and the free energy (internal energy) of the free oscillator. For our model, they read, respectively

$$F_{cl} = -\mu + \frac{1}{\pi}\int_0^\infty \mathrm{d}\omega F_f(\omega, T)\mathrm{Im}\left[\frac{d}{d\omega}\ln\chi_{cl}(\omega)\right], \tag{2.29}$$

and

$$U_{cl} = -\mu + \frac{1}{\pi}\int_0^\infty \mathrm{d}\omega U_f(\omega, T)\mathrm{Im}\left[\frac{d}{d\omega}\ln\chi_{cl}(\omega)\right]. \tag{2.30}$$

Here, $F_f(\omega, T) = T\ln[2\sinh(\omega/(2T))]$ and $U_f(\omega, T) = (\omega/2)\coth(\omega/(2T))$. The extra μ terms stem from the Lagrange multiplier enforcing the large-N constraint [110].

The entropy $S_{cl} = (U_{cl} - F_{cl})/T$ can be calculated simply by inserting Eq. (2.27) into Eqs. (2.29) and (2.30) and computing the resulting integral. For the dynamical clusters ($s < s_c$), the low-temperature entropy behaves as

$$S_{cl} = B_\zeta \alpha s \omega_c^{1-\zeta}\frac{T^\zeta}{\epsilon_0}, \tag{2.31}$$

where B_ζ is a ζ-dependent constant. At higher temperatures (greater than $T^* \sim \epsilon_0^{1/\zeta}\omega_c^{1-1/\zeta}$), the entropy becomes weakly dependent on T. [‡].

[‡]For $\zeta < 1/2$ it has a logarithmic T-dependence, while for $\zeta > 1/2$ its dependence on T is even weaker [110]

In the low-T limit, the specific heat $C_{cl} = T(\partial S_{cl}/\partial T)$ thus behaves as

$$C_{cl} = B_\zeta \zeta \alpha s \omega_c^{1-\zeta} \frac{T^\zeta}{\epsilon_0}. \tag{2.32}$$

3.2. COMPLETE SYSTEM. After discussing the behavior of a single percolation-cluster, we now turn to the full diluted lattice model. The low-energy density of states of the dynamic clusters $\rho_{dy}(\epsilon) = \sum_{s<s_c} n_s \delta(\epsilon - \epsilon_0(s))$ is obtained combining the single-cluster result Eq. (2.18) with the cluster-size distribution Eq. (2.8), yielding

$$\rho_{dy}(\epsilon) = A_\zeta^{-1} \left(x^{-1} - 1\right) \frac{n_{s(\epsilon)} s_c}{\omega_c} \left(\frac{\epsilon}{\omega_c}\right)^{(1-2x)/x}, \tag{2.33}$$

where $s(\epsilon)$ is the size of a cluster with renormalized distance ϵ from criticality [which can be obtained inverting Eq. (2.18)]. Notice that ρ_{dy} shows no dependence on ϵ in the case $\zeta < 1/2$. In particular, it does not diverge with $\epsilon \to 0$, in contrast to the case $\zeta > 1/2$.

We now discuss the physics at the percolation transition, starting with the total magnetization m. We have to distinguish the contributions m_{dy} from dynamical clusters, m_{st} from frozen finite-size clusters, and m_∞ from the infinite percolation cluster, if any. For zero ordering field H_z, m_{dy} vanishes, because the dynamic clusters fluctuate between up and down. The frozen finite-size clusters individually have a non-zero magnetization, but it sums up to zero ($m_{st} = 0$), because they do not align coherently for $H_z = 0$. Hence, the only coherent contribution to the total magnetization is m_∞. Since the infinite cluster is long-range ordered for small transverse field $h_x < h_\infty(\alpha)$, its magnetization is proportional to the number P_∞ of sites in the infinite cluster, giving

$$m = m_\infty \sim P_\infty(p) \sim \begin{cases} |p - p_c|^{\beta_c} & (\text{for } p < p_c), \\ 0 & (\text{for } p > p_c). \end{cases} \tag{2.34}$$

The magnetization critical exponent β is therefore given by its classical lattice percolation value β_c. In response to an infinitesimally small ordering field H_z, the frozen finite-size clusters align at zero temperature, leading to a jump in $m(H_z)$ at $H_z = 0$. The magnitude of the jump is given by $m_{st} = \sum_{s>s_c} n_s$. At the percolation threshold, $m_{st} \approx (1 - p_c)s_c^{2-\tau_c}$, and it vanishes exponentially for both $p \to 0$ and $p \to 1$. The total magnetization in an infinitesimal field (given by $m_\infty + m_{st}$) is analytic at $p = p_c$, and only clusters with sizes below s_c are not polarized.

To estimate the contribution m_{dy} of the dynamic clusters, we integrate the magnetization of a single cluster Eq. (2.28) over the DOS given in Eq. (2.33). For $\zeta > 1/2$, we find that

$$m_{dy} = C_\zeta n_{s_c} s_c^2 \left(\frac{H_z s_c}{\omega_c}\right)^{3(1-\zeta)/(1+\zeta)}, \tag{2.35}$$

where n_{s_c} is the density of critical clusters, and $C_\zeta = A_\zeta^{-3\zeta/(1+\zeta)}\zeta/(2\zeta - 1)$. For $\zeta < 1/2$, the integration gives

$$m_{dy} = \frac{n_{s_c} s_c^2}{A_\zeta}\left(\frac{s_c H_z}{\omega_c}\right)\left[1 + \ln\left(\frac{\theta_0}{(A_\zeta \omega_c s_c^2 H_z^2)^{1/3}}\right)\right], \tag{2.36}$$

where θ_0 is a cut-off energy.

Because the three contributions to the magnetization have different field-dependence, the system shows unconventional hysteresis effects. The infinite cluster has a regular hysteresis loop (for $p < p_c$), the finite-size frozen clusters do not show hysteresis, but they contribute jumps in $m(H_z)$ at $H_z = 0$, and the dynamic clusters contribute a continuous but singular term (see Fig. 3.1).

The low-temperature susceptibility is dominated by the contribution χ_{st} of the static clusters, with each one adding a Curie term of the form $s(s - s_c)/T$. Summing

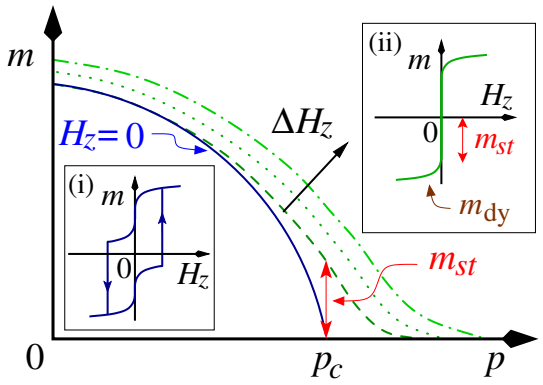

Figure 3.1: (Color online) The magnetization as a function of dilution p for different ordering field H_z at absolute zero. The solid line is the magnetization at $H_z = 0$ (The contribution of the infinite cluster only). The dashed line is for an infinitesimal field and the remaining ones represents stronger fields. Insets dysplay the histerisis curves in the (i) ordered and (ii) disordered phases.

over all static clusters, close to the percolation threshold, we find that

$$\chi_{st} \sim \sum_{s>s_c} n_s \frac{s(s-s_c)}{T} \sim \frac{1}{T}|p-p_c|^{-\gamma_c}. \tag{2.37}$$

For $p \to 0$ and $p \to 1$, the prefactor of the Curie term vanishes exponentially. The infinite cluster contribution χ_∞ remains finite (per site) for $T \to 0$, because the infinite cluster is in the ordered phase.

To determine the contribution χ_{dy} of the dynamical clusters, we integrate the single-cluster susceptibility Eq. (2.26) over the low-energy DOS in Eq. (2.33). For $\zeta > 1/2$, this gives

$$\chi_{dy} = C'_\zeta \frac{n_{s_c} s_c^3}{\omega_c} \left(\frac{T}{\omega_c}\right)^{1-2\zeta}, \tag{2.38}$$

with $C'_\zeta = A_\zeta^{-2\zeta}[\zeta/(2\zeta-1)]$. For $\zeta < 1/2$, we find

$$\chi_{dy} = A_\zeta^{-1} \frac{n_{s_c} s_c^3}{\omega_c} \left[1 + \ln\left(\frac{\theta_0}{(A_\zeta \omega_c T)^{1/2}}\right)\right]. \tag{2.39}$$

The retarded susceptibility of the fluctuating clusters can be obtained by integrating the single-cluster susceptibility Eq. (2.27) over the distribution Eq. (2.33), this leads to

$$\mathrm{Im}\,\chi_{dy}(\omega) = D_\zeta \frac{n_{s_c} s_c^3}{\omega_c} \left|\frac{\omega}{\omega_c}\right|^{1-2x} \mathrm{sgn}(\omega), \tag{2.40}$$

with $D_\zeta = A_\zeta^{-1}(\frac{1}{x}-1)\pi \sin(\theta(\frac{1}{x}-2))/[\sin(\frac{\pi}{x})(\pi(1-\zeta))^{\frac{1}{x}-2}]$. We notice that $\mathrm{Im}\,\chi_{dy}$ has no ω-dependence for $\zeta < 1/2$.

Finally, we consider the heat capacity. The dynamical cluster contribution can be obtained by summing the single-cluster heat capacity Eq. (2.32) over $\rho_{dy}(\epsilon)$, yielding $C_{dy} \sim n_{s_c} s_c \,(T/\omega_c)^{1-\zeta}$ for $\zeta > 1/2$ and $C_{dy} \sim n_{s_c} s_c \,(T/\omega_c)^{\zeta}$ for $\zeta < 1/2$.

4. BEYOND THE LARGE-N LIMIT: SCALING APPROACH

In the last subsection, we have studied the percolation quantum phase transition of the diluted sub-Ohmic rotor model Eq. (2.4) in the large-N limit. Let us now go beyond the large-N limit and consider the rotor model with a finite number of components as well as the quantum Ising model Eq. (2.2).

We begin by analyzing a single percolation cluster of s sites. For strong dissipation $\alpha > \alpha_\infty$ (or weak fluctuations $h_x < h_\infty$), this cluster can be treated as a compact object that fluctuates in (imaginary) time only. As pointed out in Sec. 2.3, in the presence of sub-Ohmic dissipation, such a cluster undergoes a continuous quantum phase transition from a fluctuating to a localized phase as a function of increasing dissipation strength or, equivalently, cluster size s.

Even though the critical behavior of this quantum phase transition is not exactly solvable, we can still write down a scaling description of the cluster free energy

$$F_{cl}(r, H_z, T) = b^{-1} F_{cl}(r b^{1/(\nu_s z_s)}, H_z b^{y_s}, Tb) \tag{2.41}$$

where $r = \alpha_s - \alpha_c = (s - s_c)\alpha$ is the distance from criticality, b is an arbitrary scale factor, and $\nu_s z_s$ and y_s are the critical exponents of the single-cluster quantum phase transition. (We use a subscript s to distinguish the single-cluster exponents from those associated with the percolation quantum phase transition of the diluted lattice.)

Normally, one would expect the two exponents $\nu_s z_s$ and y_s to be independent. However, because the sub-Ohmic damping corresponds to a long-range interaction in time, the exponent η takes the mean-field value $2 - \zeta$ for all ζ [83, 111, 112]. This also fixes the exponent y_s in Eq. (2.41) to be $y_s = (1 + \zeta)/2$. Thus, there is only one independent exponent in addition to ζ; in the following we choose the susceptibility exponent γ_s. This implies, via the usual scaling relations, that the correlation time exponent is given by $\nu_s z_s = \gamma_s/\zeta$.

The values of the cluster exponents in the large-N case of Sec. 3. are given by $\gamma_s = \zeta/(1-\zeta)$ and $\nu_s z_s = 1/(1-\zeta)$. In the general case of finite-N rotors and for the quantum Ising model, they can be found numerically. Notice the scaling form of the free energy Eq. (2.41) applies to bath exponents $\zeta > 1/2$. For $\zeta < 1/2$, the single-cluster critical behavior is mean-field-like.

The behavior of single-cluster observables close to the (single-cluster) quantum critical point can now be obtained by taking the appropriate derivatives of the free energy Eq. (2.41). For example, the static magnetic susceptibility at $T = 0$ and $H_z = 0$ behaves as

$$\chi(r, \omega = 0) \sim r^{-\gamma_s} \ . \tag{2.42}$$

Using this result, we can derive a generalization of the probability distribution $\rho_{dy}(\epsilon)$ of the inverse static susceptibilities $\epsilon = \chi^{-1}$. We find

$$\rho_{dy}(\epsilon) = \int_1^{s_c} \mathrm{d}s \, n_s \, \delta\left[\epsilon - c(s_c - s)^{\gamma_s}\right] \sim n_{s_c} \, \epsilon^{(1-\gamma_s)/\gamma_s} \tag{2.43}$$

right at the percolation threshold. In the large-N limit, $\gamma_s = \zeta/(1-\zeta)$ implying $\rho_{dy}(\epsilon) \sim \epsilon^{(1-2\zeta)/\zeta}$ in agreement with the explicit result in Eq. (2.33).

Let us now discuss how the properties of the percolation quantum phase transition in the general case differ from those obtained in the large-N limit in Sec. 3.2. We focus on the case $\zeta > 1/2$. If the single-cluster critical behavior is of mean-field type ($\zeta < 1/2$), the functional forms of the results in Sec. 3.2 are not modified at all. The total magnetization is the sum of the magnetization m_∞ of the infinite percolation cluster, m_{st} stemming from the large ($s > s_c$) frozen percolation clusters, and m_{dy} provided by the dynamic clusters having $s < s_c$. Both m_∞ and m_{st} are completely independent of the single-cluster critical behavior. The behavior of the spontaneous (zero-field) magnetization across the percolation transition in the general case is thus identical to that of the large-N limit [see Eq. (2.34) and Fig. 3.1]. In contrast, the magnetization–magnetic field curve of the dynamic clusters does depend on the value

of γ_s. Integrating the single cluster-magnetization of all dynamic clusters [in analogy to Eq. (2.28)] gives

$$m_{dy} \sim H_z^{[1-\zeta+2\zeta/\gamma_s]/(1+\zeta)}. \tag{2.44}$$

In the large-N limit, this recovers the result Eq. (2.35), as expected.

The low-temperature susceptibility can be discussed along the same lines. The contributions χ_∞ and χ_{st} do not depend on the single-cluster critical behavior. Integrating the single-cluster susceptibility over all dynamic clusters using (2.43) yields (at $p = p_c$)

$$\chi_{dy} \sim T^{(1-\gamma_s)\zeta/\gamma_s} \ . \tag{2.45}$$

If we use the large-N value of γ_s, we reproduce Eq. (2.38).

The scaling ansatz Eq. (2.41) for the single-cluster free energy thus allows us to discuss the complete thermodynamics across the percolation quantum phase transition. Dynamic quantities can be analyzed in the same manner. For example, the scaling form of the single-cluster dynamic susceptibility reads

$$\chi_{cl}(r, H_z, T, \omega) = b^{2y_s-1}\chi_{cl}(rb^{1/(\nu_s z_s)}, H_z b^{y_s}, Tb, \omega b) \tag{2.46}$$

The contribution of the fluctuating clusters to the low-temperature dynamic susceptibility can be found by integrating the single-cluster contribution over the distribution Eq. (2.43). This leads to

$$\mathrm{Im}\,\chi_{dy}(\omega) \sim |\omega|^{(1-\gamma_s)\zeta/\gamma_s}\,\mathrm{sgn}(\omega) \ . \tag{2.47}$$

In the large-N limit this corresponds to $\mathrm{Im}\,\chi_{dy}(\omega) \sim |\omega|^{1-2\zeta}\,\mathrm{sgn}(\omega)$ in agreement with Eq. (2.40) for $\zeta > 1/2$.

In summary, even though the critical behavior is not exactly solvable for finite-N rotors and quantum Ising models, we can express the properties of the percolation

quantum phase transition in terms of a single independent exponent of the single-cluster problem (which can be found, e.g., numerically).

5. CONCLUSIONS

We have investigated the effects of local sub-Ohmic dissipation on the quantum phase transition across the lattice percolation threshold of diluted quantum Ising and rotor models. Experimentally, such local dissipation (with various spectral densities) can be realized, e.g., in molecular magnets weakly coupled to nuclear spins [105, 106] or in magnetic nanoparticles in an insulating host [107]. Further potential applications include diluted two-level atoms in optical lattices coupled to an electromagnetic field, random arrays of tunneling impurities in crystalline solids or, in the future, large sets of coupled qubits in noisy environments.

As even a single spin or rotor undergoes a localization quantum phase transition for sufficiently strong sub-Ohmic damping, the quantum dynamics of large percolation clusters in the diluted lattice freezes completely. The coexistence of these frozen clusters which effectively behave as classical magnetic moments and smaller fluctuating clusters, if any, leads to unusual properties of the percolation quantum phase transition. In this final section, we put our results into broader perspective.

Let us compare the three different quantum phase transitions separating the paramagnetic and ferromagnetic phases [transitions (i), (ii), and (iii) in Fig. 2.1]. The generic transition (i) occurs as a function of transverse field or dissipation strength for $p < p_c$. This transition is smeared by the mechanism of Ref. [46] because rare vacancy-free spatial regions can undergo the quantum phase transition independently from the bulk system. For $p < p_c$, these rare regions are weakly coupled leading to magnetic long-range order instead of a quantum Griffiths phase [47, 98].

In contrast, the percolation transitions (ii) and (iii) are not smeared but sharp. The reason is that different percolation clusters are completely decoupled for $p > p_c$. Thus, even if some of these clusters have undergone the (localization) quantum phase transition and display local order, their local magnetizations do not align, leading to

an incoherent contribution to the global magnetization. Deviations from a pure percolation scenario change this conclusion. If the interaction has long-range tails (even very weak ones), different frozen clusters will be coupled, and their magnetizations align coherently. This leads to a smearing of the dilution-driven transition analogous to that of the transition (i). However, if the long-range tail of the interaction is weak, the effects of the smearing become important at the lowest energies only. What is the difference between the percolation transitions (ii) and (iii) in Fig. 2.1? If all percolation clusters are frozen [transitions (iii)] low-temperature observables behave purely classically. If large frozen and smaller dynamic clusters coexist [transitions (ii)] quantum fluctuations contribute to the observables at the percolation transition.

We now compare the case of sub-Ohmic dissipation considered here to the cases of Ohmic and super-Ohmic dissipation as well as the dissipationless case. To do so, we need to distinguish the quantum Ising model and the rotor model.

The percolation transitions of the dissipationless and super-Ohmic rotor models display conventional critical behavior, but with critical exponents that differ from the classical percolation exponents [109]. (This holds for the particle-hole symmetric case in which complex Berry phase terms are absent from the action [90]). In the Ohmic rotor model, the percolation transition displays activated scaling as at infinite-randomness critical points [109].

For the diluted quantum Ising model, the percolation transition displays activated scaling already in the dissipationless [89] and super-Ohmic cases [98]. In the presence of Ohmic dissipation, sufficiently large percolation clusters can undergo the localization transition independently from the bulk. The resulting percolation transition [103] is similar to the one discussed in the present paper, it shows unusual properties due to an interplay of frozen and dynamic percolation clusters.

All these results suggest that quantum phase transitions across the lattice percolation threshold can be classified analogously to generic disordered phase transitions, [30, 91] (provided the order parameter action does not contain complex terms).

If a single finite-size percolation cluster is below the lower critical dimension of the problem, it can not undergo a phase transition independent of the bulk system. The resulting percolation transition displays conventional critical behavior (this is the case for the dissipationless and super-Ohmic rotor models). If a single finite-size cluster can undergo the transition by itself (i.e., it is above the lower critical dimension of the problem), the resulting percolation transition is unconventional with some observables behaving classically while others are influenced by quantum fluctuations. This scenario applies to the sub-Ohmic models studied in this paper as well as the Ohmic quantum Ising model. Finally, if a single percolation cluster is right at the lower critical dimension (but does not undergo a phase transition), the percolation quantum phase transition shows activated critical behavior. This scenario applies to the dissipationless quantum Ising model as well as the Ohmic quantum rotor model.

6. ACKNOWLEDGEMENTS

This work has been supported in part by the NSF under grant no. DMR-0906566, by FAPESP under Grant No. 2010/ 03749-4, and by CNPq under grants No. 590093/2011-8 and No. 302301/2009-7.

III. MONTE-CARLO SIMULATIONS OF THE DISSIPATIVE RANDOM TRANSVERSE-FIELD ISING CHAIN

Manal Al-Ali, and Thomas Vojta

[1]*Department of Physics, Missouri University of Science & Technology, Rolla, MO 65409*

ABSTRACT*

We study the influence of Ohmic dissipation on the random transverse-field Ising chain by means of large-scale Monte-Carlo simulations. To this end, we first map the Hamiltonian onto a classical Ising model with long-range $1/\tau^2$ interaction in the time-like direction. We then apply the highly efficient cluster algorithm proposed by Luijten and Blöte for system with long-range interactions. Our simulations show that Ohmic dissipation destroys the infinite-randomness quantum critical point of the dissipationless system. Instead, the quantum phase transition between the paramagnetic and ferromagnetic phases is smeared. We compare our results to recent predictions of a strong-disorder renormalization group approach, and we discuss generalizations to higher dimensions as well as experiments.

*All of this section is reproduced from the manuscript (e-printed version, arXiv:submit/0768523).

1. INTRODUCTION

Dissipation and disorder are two phenomena that can qualitatively change the properties of quantum phase transitions. Dissipation alone can cause a finite-size quantum system to undergo a transition. For example, the spin-boson model, a two-level system coupled to a dissipative bath of harmonic oscillators, undergoes a quantum phase transition from a fluctuating phase to a localized phase as the dissipation strength increases. [27, 28] Similar quantum phase transitions occur in other quantum impurity models.[61] In extended systems, the addition of dissipation can change the universality class of the transition. [113] Dissipation plays a particularly important role for quantum phase transitions in metallic systems because the order parameter fluctuations are damped by the coupling to gapless particle-hole excitations. [17, 19, 21]

Quenched disorder comprises impurities, defects, and other types of imperfections. It can change the order of a transition from first-order to continuous, [114, 115, 116, 117] and it can modify the critical behavior, resulting in a different universality class. [33] Moreover, at some quantum phase transitions, disorder leads to exotic exponential scaling [39, 40] and to quantum Griffiths singularities [86, 118] in the vicinity of the transition point (see Refs. [30, 31] for recent reviews).

If disorder and dissipation occur simultaneously in a system undergoing a quantum phase transition, even stronger effects can be expected. The dissipative random transverse-field Ising chain is a prototypical microscopic model for studying these phenomena. Due to the disorder, this system contains rare large strongly coupled regions that are locally in the ferromagnetic phase while the bulk system is still paramagnetic. Each of these locally ferromagnetic regions acts as a quantum two-level system. In the presence of (Ohmic) dissipation, the quantum dynamics of sufficiently large such regions completely freezes as they undergo the localization transition of

the Ohmic spin-boson model. Because each rare region freezes independently from the rest of the system, the global quantum phase transition is smeared. [46]

Going beyond these heuristic arguments, Schehr and Rieger [96, 97] developed a numerical strong-disorder renormalization group approach to the dissipative random transverse-field Ising chain. They confirmed the smeared transition scenario but focused on the pseudo-critical point found at intermediate energies. Later, Hoyos and Vojta [47, 98] developed a complete analytic theory by means of a slightly modified renormalization group method. This theory becomes controlled in the strong-disorder limit but its validity for weaker disorder requires independent verification.

In the present paper, we therefore perform large-scale Monte-Carlo simulations of the dissipative random transverse-field Ising chain. Our goals are to test the predictions of the strong-disorder renormalization group theory of Refs. [47, 98] and to determine to what extent it applies to moderately or even weakly disordered systems. Our paper is organized as follows. We define the quantum Hamiltonian in Sec. 2. and map it onto an anisotropic two-dimensional classical Ising model. In Sec. 3., we describe our simulation method and report the numerical results. We conclude in Sec. 4. by discussing generalizations to higher dimensions as well as experimental applications.

2. MODEL AND QUANTUM-TO-CLASSICAL MAPPING

The Hamiltonian of the dissipative random transverse-field Ising chain consists of three parts,

$$H = H_I + H_B + H_C \ . \tag{3.1}$$

H_I denotes the Hamiltonian of the usual, dissipationless transverse-field Ising model,

$$H_I = -\sum_i J_i \sigma_i^z \sigma_{i+1}^z - \sum_i h_i \sigma_i^x \tag{3.2}$$

where σ_i^z and σ_i^x are Pauli matrices representing the spin at lattice site i. J_i is the nearest-neighbor interaction between sites i and $i+1$ while h_i is the transverse field acting on site i.

H_B represents the Hamiltonians of independent harmonic oscillator baths (one for each site); it is given by

$$H_B = \sum_{k,i} \omega_{k,i} \left(a_{k,i}^\dagger a_{k,i} + \frac{1}{2} \right) \ . \tag{3.3}$$

Here, $\omega_{k,i}$ is the frequency of the k-th oscillator coupled to the spin at site i, and $a_{k,i}$ and $a_{k,i}^\dagger$ are the usual annihilation and creation operators.

The coupling between the spins and the dissipative baths is given by H_C which reads

$$H_C = \sum_i \sigma_i^z \sum_k \lambda_{k,i} \left(a_{k,i}^\dagger + a_{k,i} \right) , \tag{3.4}$$

with $\lambda_{k,i}$ denoting the strength of the interaction.

The character and strength of the dissipation provided by the oscillator baths is contained in their spectral densities

$$\mathcal{E}_i(\omega) = \pi \sum_k \lambda_{k,i}^2 \delta \left(\omega - \omega_{k,i} \right) \ . \tag{3.5}$$

Power-law spectral densities are of particular interest; they can be parameterized as

$$\mathcal{E}_i(\omega) = \frac{\pi}{2}\alpha_i \omega_c^{1-s}\omega^s \quad (\omega < \omega_c) \ . \tag{3.6}$$

Here, ω_c is a high-energy cutoff, and α_i is a dimensionless measure of the dissipation strength. The value of the exponent s determines the qualitative character of the dissipation. Superohmic baths ($s > 1$) are weak, they cannot induce a localization transition of a single spin. The experimentally important Ohmic dissipation ($s = 1$) constitutes the marginal case: If the dissipation strength α is sufficiently large, an Ohmic baths can localize a single spin via a Kosterlitz-Thouless impurity quantum phase transition. Subohmic dissipation ($s < 1$) is even stronger, it also induces a single-spin localization transition. In this paper, we mostly consider Ohmic dissipation, but we will comment on the other types in the concluding section. Moreover, we restrict ourselves to the experimentally most interesting case of the bath cutoff ω_c being the largest energy, $\omega_c \gg h_i, J_i$.

As we are interested in the disordered, random version of the Hamiltonian (3.1), we allow the interactions J_i, the transverse fields h_i, and the dissipation strengths α_i to be independent random variables.

To apply our Monte-Carlo method, we now map the one-dimensional quantum Hamiltonian (3.1) onto a two-dimensional classical Ising model. This can be done using standard techniques, for example using a Feynman path integral [79] representation of the partition function or a transfer matrix method. [3] After integrating out all the bath oscillators, we arrive at the following effective classical Hamiltonian:

$$\begin{aligned} H_{cl} = \ & - \sum_{i,\tau} J_i^x S_{i,\tau} S_{i+1,\tau} - \sum_{i,\tau} J_i^\tau S_{i,\tau} S_{i,\tau+1} \\ & - \sum_{i,\tau,\tau'} \frac{\bar{\alpha}_i}{|\tau - \tau'|^{1+s}} S_{i,\tau} S_{i,\tau'} \ . \end{aligned} \tag{3.7}$$

Here, $S_{i,\tau} = \pm 1$ are classical Ising variables, i indexes the space direction and τ indexes the imaginary time-like direction. The long-range interaction in the time direction in the last term results from integrating out the dissipative baths. The coefficients J_i^x, J_i^τ, and $\bar{\alpha}_i$ are determined by the parameters of the original quantum Hamiltonian. In the following, we treat these coefficients as fixed constants and drive the transition by varying the classical temperature T (which is not identical to the temperature of the original quantum system which is zero).

3. MONTE-CARLO SIMULATIONS

3.1. METHOD AND PARAMETERS. We performed large-scale Monte Carlo simulations of the classical Hamiltonian (3.7) for the case of Ohmic dissipation, $s = 1$. To overcome the critical slowing down near the phase transition, we used the Wolff cluster algorithm. [119]

The long-range interaction in the time-like direction (last term of the classical Hamiltonian (3.7)) poses additional problems. A straightforward implementation of the Wolff algorithm for this Hamiltonian is not very efficient. When building a cluster, all spins interacting with a given site need to be considered for addition to the cluster, not just the nearest neighbor sites as in the case of short-range interactions. As a result, the numerical effort scales quadratically with the number of sites in the time-like direction rather then linearly. This problem is overcome by a clever version of the Wolff algorithm due to Luijten and Blöte [120] that leads to linear scaling of the numerical effort with system size, independent of the interaction range. We used this algorithm for all our simulations (except for a few test runs in which we compared its results to that of straightforward implementations of the Wolff and Metropolis algorithms).

We simulated systems with linear sizes of up $L = 10000$ in space direction and $L_\tau = 6000$ in time direction. The results are averages over large numbers of disorder realizations (from 200 to 2000 depending on system size). Each sample was equilibrated using 200 Monte-Carlo sweeps (spin flips per site). After that, observables were measured once every sweep for a total measurement period of 200 to 10000 sweeps, again depending on system size.

Quenched disorder was introduced into our simulations by making the interactions J_i^x in the space direction independent random variables governed by a binary

probability distribution

$$P(J^x) = (1-p)\,\delta(J^x - 1) + p\,\delta(J^x - c) \tag{3.8}$$

where p is the concentration of weak bonds and $0 < c \leq 1$ is their interaction energy. We fixed these parameters at $p = 0.8$ and $c = 0.25$. The interactions in time direction were taken to be uniform $J_i^\tau \equiv J^\tau$, as were the dissipation strengths $\bar{\alpha}_i \equiv \bar{\alpha}$.

To test the predictions of the strong-disorder renormalization group theory, [47, 98] we considered two different parameter sets. (i) Strong dissipation, $\bar{\alpha} = 1$. In this case, we neglected the short-range part of the interaction in the time direction (i.e., we set $J^\tau = 0$) as it is irrelevant for the critical behavior. (ii) Weak dissipation. To study the crossover from the infinite-randomness criticality of the dissipationless model, we set $J^\tau = 1$ and varied $\bar{\alpha}$ from 0 to 0.5. All simulations were performed on the Pegasus II computer cluster at Missouri S&T.

3.2. RESULTS FOR STRONG DISSIPATION. In this section we discuss results for the case $\bar{\alpha} = 1$ and $J^\tau = 0$. To test our implementation of the Luijten-Blöte algorithm, [120] we first considered a clean system with zero concentration of weak bonds ($p = 0$). We analyzed the finite-size scaling behavior of the magnetization m, the magnetic susceptibility χ as well as the Binder cumulant $g = 1 - \langle m^4 \rangle / (3\langle m^2 \rangle^2)$ close to the transition temperature $T_c^0 \approx 3.98$. Results for the Binder cumulant and the magnetization are presented in Figs. 3.1 and 3.2. Both quantities display high-quality scaling as does the susceptibility (not shown). The resulting critical exponents, $\nu = 0.638$, $z = 1.98$, $\beta = 0.319$, and $\gamma = 1.27$ agree with literature values for the dissipative transverse-field Ising chain. [113]

We note that the correlation length exponent violates the Harris criterion [33] $d_\perp \nu > 2$. Here, $d_\perp = 1$ is the number of "random dimensions" which differs from the total dimensionality $d = 2$ of the classical model (3.7) because the disorder is perfectly correlated in the time-like direction. The violation of Harris' inequality suggests that

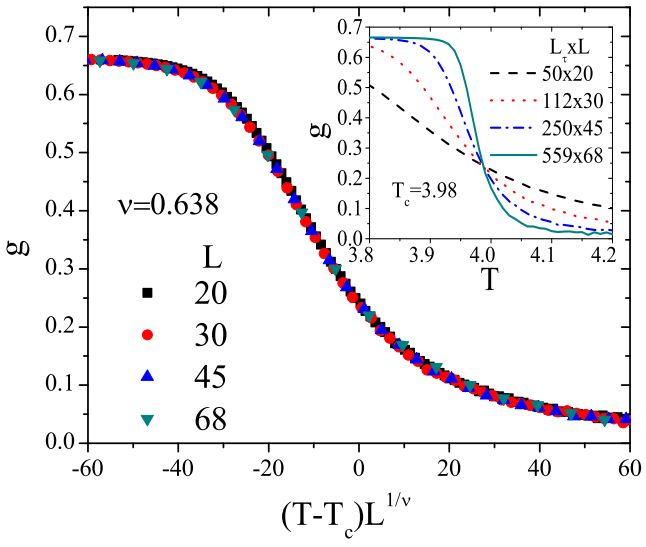

Figure 3.1: (Color online) Finite-size scaling of the Binder cumulant g for the classical Hamiltonian (3.7) with $\bar{\alpha} = 1$ and $J^\tau = 0$ in the clean limit $p = 0$ giving a correlation length critical exponent $\nu = 0.638$. The inset shows the raw data which give a high-quality crossing at $T_c^0 \approx 3.98$. The sample shapes (L vs. L_τ) reflect the dynamical exponent value $z = 1.98$.

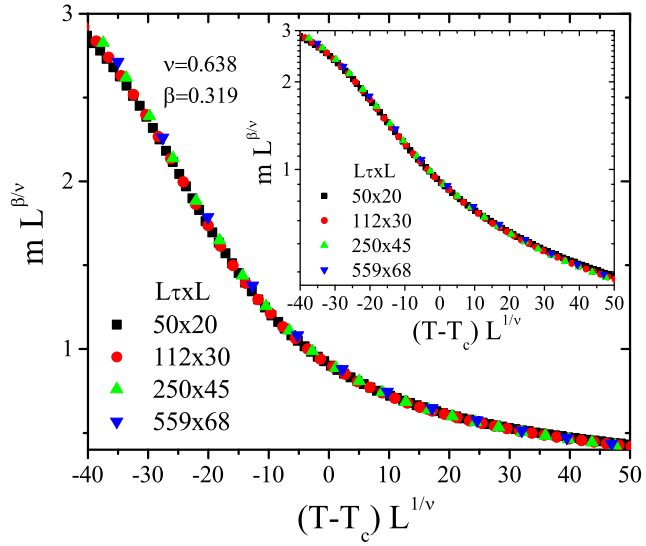

Figure 3.2: (Color online) Finite-size scaling of the magnetization m for the classical Hamiltonian (3.7) with $\bar{\alpha} = 1$ and $J^\tau = 0$ in the clean limit $p = 0$ giving an order parameter critical exponent $\beta = 0.319$. The inset shows the same data on a logarithmic scale.

weak disorder is a relevant perturbation at the clean critical point; the character of the transition is thus expected to change upon the introduction of disorder.

In addition to providing a test of our numerical algorithm, the clean system simulations also give us a value for the upper Griffiths temperature T_u for later use in the analysis of the disordered case. The upper Griffiths temperature is the temperature above which no (rare) locally ordered regions can exist in the disordered system. For the binary disorder distribution (3.8), the upper Griffiths temperature is identical to the critical temperature of an impurity-free system ($p = 0$). Thus, in our case $T_u = T_c^0 \approx 3.98$.

We now turn to our simulations of the disordered case, using $p = 0.8$ and $c = 0.25$ in the binary distribution (3.8). To establish the smeared character of the phase transition, we analyzed the temperature dependence of the magnetization. According to the theoretical predictions, [45, 46] the magnetization is expected to develop an exponential tail of the form

$$m = m_0 \exp[-(T_c^0 - T)^{-\nu}] \tag{3.9}$$

towards the upper Griffiths temperature $T_u = T_c^0$. Here, ν is the correlation length exponent of the clean system. This tail forms because sufficiently large individual rare regions undergo the phase transition independently at different values of the tuning parameter. (After the quantum-to-classical mapping, these rare regions correspond to "strips" of finite width in the space direction.) To see this phenomenon in the simulations of finite-size systems requires a careful choice of the simulation parameters. In particular, the system size L_τ in the time-like direction needs to be very large to allow for sharp transitions of the individual rare regions to occur. Note that the smeared transition in the original quantum Hamiltonian (3.1) occurs only in the zero-temperature limit which corresponds to the limit $L_\tau \to \infty$ in the classical model (3.7). In contrast, the system size L is space direction is not very important

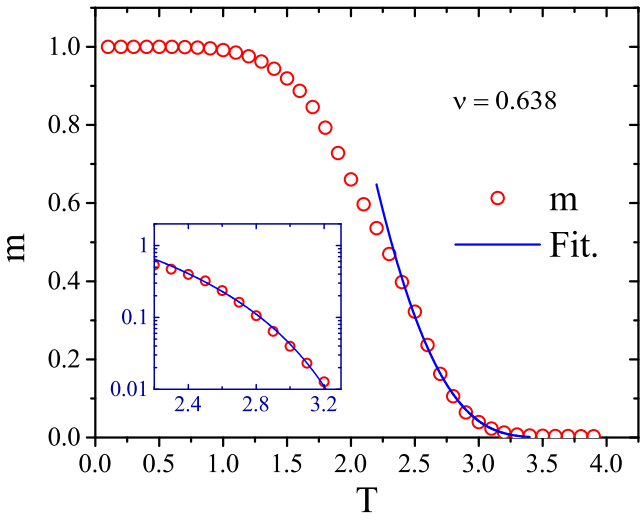

Figure 3.3: (Color online) Magnetization m vs temperature T for the classical Hamiltonian (3.7) with $p = 0.8$, $c = 0.25$, $\bar{\alpha} = 1$ and $J^\tau = 0$ for a system of size $L = 50, L_\tau = 6000$, averaged over 200 disorder realizations. m develops a pronounced tail towards $T_c^0 = 3.98$. The solid line is a fit to (3.9). The semi-log plot of the same data in the inset shows that the theoretical prediction fits the tail region for almost two orders of magnitude in m.

because the tail of the smeared transition is produced by finite-size rare regions (and the spatial correlation length remains finite).

Figure 3.3 shows the magnetization as a function of temperature for a system of size $L = 50, L_\tau = 6000$, averaged over 200 disorder realizations. The data display a pronounced tail towards the upper Griffiths temperature $T_u = T_c^0$. We have compared different system sizes to ensure that this tail is *not* the result of any remaining finite-size effects. To compare with the theoretical predictions, we fit the magnetization in the tail region (temperatures above the inflection point at $T \approx 2.3$) to the exponential form (3.9). The numerical data follow the prediction for almost two orders of magnitude in m (temperatures between 2.3 and 3.2). At higher temperatures, the numerical magnetization value is dominated by Monte-Carlo noise and thus saturates at a roughly temperature-independent value. (To suppress this effect, one would need to use even larger system sizes.)

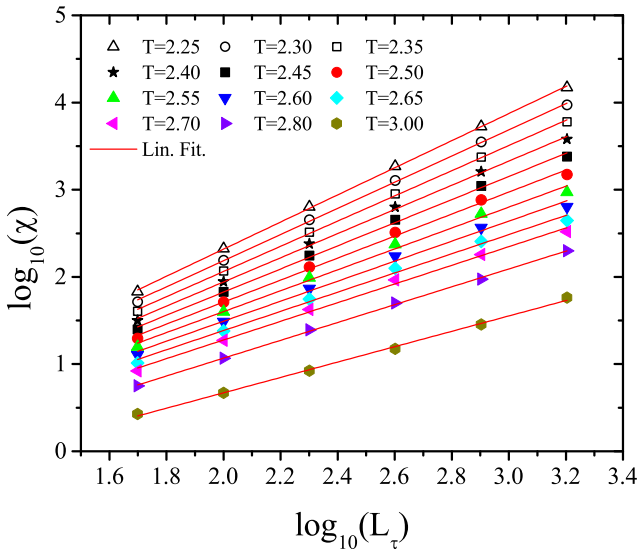

Figure 3.4: (Color online) Susceptibility χ vs system size L_τ for the classical Hamiltonian (3.7) with $p = 0.8$, $c = 0.25$, $J^\tau = 0$, and $\bar{\alpha} = 1$ at different values of the classical temperature T. The spatial system size is $L = 3000$. The solid lines are fits to the power-law (3.10).

In addition to the magnetization, we also studied the magnetic susceptibility in the tail region of the smeared transition. According to the strong-disorder renormalization group theory, [47, 98] the temperature dependence of the susceptibility of the quantum Hamiltonian (3.1) is characterized by a complicated double crossover (see Fig. 3b of Ref. [98]). At higher temperatures, the physics is dominated by small clusters that cannot order (or freeze) independently. Thus, they display power-law quantum Griffiths behavior similar to the dissipationless system. At lower temperatures, the relevant clusters become large enough to undergo the localization phase transition independently, i.e., their quantum dynamics freezes. As a result, each such region makes a classical Curie contribution to the susceptibility.

Under the quantum-to-classical mapping, the (inverse) temperature in the quantum Hamiltonian (3.1) maps onto the time-like system size L_τ in the classical model (3.7). Figure 3.4 thus shows the dependence of the magnetic susceptibility χ on L_τ for several values of the classical temperature T in the tail region of the smeared transition. The data can all be fitted well by the power-law relation

$$\chi \sim L_\tau^{1-\lambda} = L_\tau^{1\pm 1/z'} \tag{3.10}$$

where λ is the usual nonuniversal Griffiths exponent (see, e.g., Ref. [30]) and z' is the corresponding dynamical exponent in the Griffiths phase. Here, the + sign in the exponent applies in the ferromagnetic Griffiths phase and the − sign in the paramagnetic Griffiths phase. For the fit curves in Fig. 3.4, λ ranges from -0.55 at $T = 2.25$ to 0.12 at $T = 3.0$.

The fact that all data in Fig. 3.4 follow (pure) power laws with a monotonously changing exponent λ suggests that our simulations are still in the transient Griffiths regime predicted by the strong-disorder renormalization group. They have not yet reached the asymptotic large-L_τ regime dominated by frozen clusters. In fact, the data at the highest classical temperature $T = 3.0$ show a slight upturn for large L_τ which may indicate the beginning of the crossover to the asymptotic regime.

3.3. CROSSOVER BETWEEN THE DISSIPATIONLESS AND DISSIPATIVE CASES. The strong-disorder renormalization group theory [47, 98] also makes detailed predictions for the crossover from the dissipationless to the dissipative behavior with increasing dissipation strength α. To investigate this crossover numerically, we first analyzed a dissipationless system by setting $\bar{\alpha} = 0$ and $J^\tau = 1$. In this case, the theory predicts a sharp transition governed by an infinite-randomness critical point. [39, 40] We confirmed this prediction by applying the methods of Ref. [121] to the case at hand, in agreement with earlier simulation results in the literature. [87] Specifically, by analyzing the finite-size scaling properties of the susceptibility, we found the critical temperature of the dissipationless system to be $T_c^{dl} \approx 1.414$ (see Fig. 3.5).

We then performed simulations for $J^\tau = 1$ and several values of the dissipation strength between $\bar{\alpha} = 0.01$ and 0.5. The resulting magnetization in the temperature range $T = 1.0$ to 3.0 is presented in Fig. 3.6. In this figure, even the magnetization of the dissipationless system ($\bar{\alpha} = 0$), which has a sharp phase transition in the

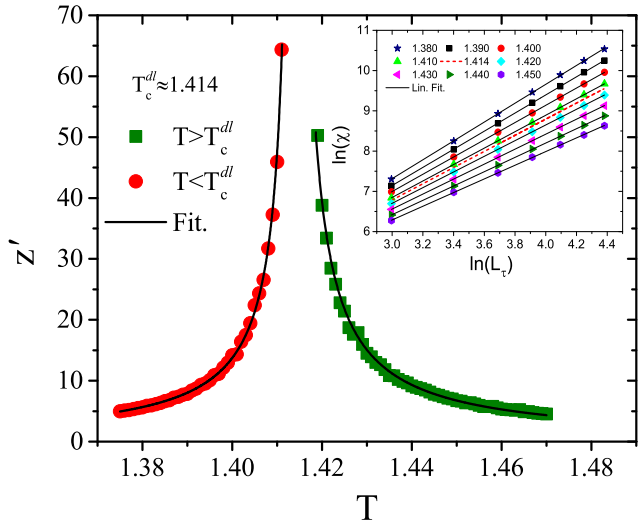

Figure 3.5: (Color online) Griffiths dynamical exponent z' vs temperature T for the classical Hamiltonian (3.7) with $p = 0.8$, $c = 0.25$, and $J^\tau = 1$ in the absence of dissipation ($\bar{\alpha} = 0$). A fit to the expected [40] power law $z' \sim |T - T_c^{dl}|^{-1}$ results in $T_c^{dl} \approx 1.414$. The inset shows the raw susceptibility data as a function of the time-like system size L_τ. The spatial system size is $L = 2000$, and the data are averaged over 1400 to 2000 disorder realizations.

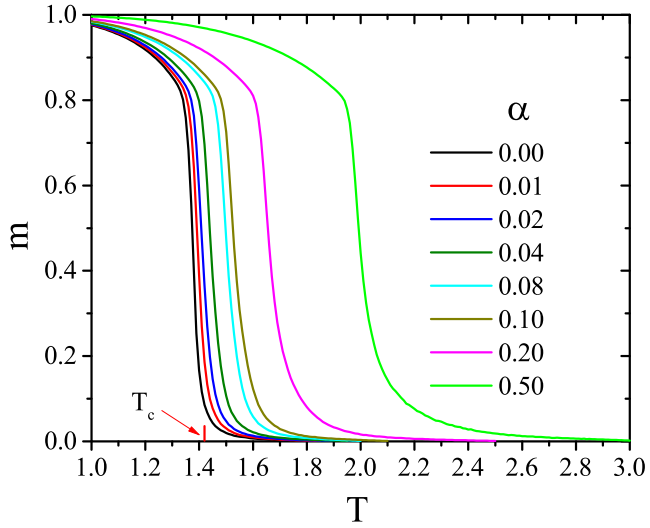

Figure 3.6: (Color online) Magnetization m vs temperature T for the classical Hamiltonian (3.7) with $p = 0.8$, $c = 0.25$, and $J^\tau = 1$ for several values of the dissipation strength $\bar{\alpha}$. The system size is $L = 200$, $L_\tau = 10000$, and the data are averaged over 500 disorder realizations. The critical temperature of the dissipationless system ($\bar{\alpha} = 0$) is $T_c^{dl} \approx 1.414$.

thermodynamic limit, shows a small "tail." It stems from the remaining finite-size effects and can thus not be completely avoided. With increasing dissipation, the magnetization tail becomes much more pronounced than this finite-size tail, again lending support to the smeared transition scenario of Refs. [47, 98].

However, a quantitative comparison with the theory of the crossover between the dissipationless and dissipative cases would require analyzing the weak-dissipation data ($\bar{\alpha} \ll 1$). For these cases, the smearing-induced magnetization tail is masked by the remaining finite-size effects and can thus not be studied quantitatively. Analogous problems also hinder the analysis of the magnetic susceptibility. We conclude that although our weak-dissipation results are in qualitative agreement with the theoretical predictions, a quantitative test of the crossover would require significantly larger systems.

4. CONCLUSIONS

To summarize, we investigated the quantum phase transition of a random transverse-field Ising chain in the presence of Ohmic dissipation. To this end, we first mapped the quantum Hamiltonian onto a classical two-dimensional Ising model with long-range ($1/\tau^2$) interactions in the time-like direction. This classical system was then studied by means of Monte-Carlo simulations using the Luijten/Blöte version of the Wolff cluster algorithm that efficiently deals with the long-range interactions.

Our results provide numerical evidence for the predictions of a recent strong-disorder renormalization group theory [47, 98] as well as earlier heuristic arguments. [46] In particular, the simulations confirm that the combined effects of disorder and dissipation lead to a destruction of the sharp quantum phase transition by smearing. This happens because different spatial regions can undergo the phase transition independently of the bulk system at different values of the tuning parameter.

For sufficiently strong dissipation (here, $\bar{\alpha} = 1$), we could quantitatively compare the simulation data with the theoretical predictions and found them in good agreement. For weak dissipation, a quantitative comparison was not possible because the dissipation-induced tail of the smeared transition is small and thus masked by the remaining finite-size effects in our simulations.

As pointed out in the introduction, the renormalization group theory [47, 98] becomes controlled in the limit of strong randomness while its applicability to weak and moderate disorder requires independent verification. The binary distribution (3.8) used in our simulations constitutes moderate disorder, because $\Delta J^x/J^x$ is of order unity but the distribution is *not* broad on a logarithmic scale. Our simulations thus show that a moderately disordered system follows the predictions of the strong-disorder theory. Moreover, because the clean system violates the Harris criterion (see Sec. 3.2) weak (bare) disorder will increase under coarse graining. This strongly suggests that the strong-disorder renormalization group theory governs the transition

for any nonzero disorder strength. A direct numerical verification for weak disorder would be computationally expensive because the crossover to the disorder-dominated behavior would occur at very large system sizes only.

Both the renormalization group theory and the present simulations address the case of one space dimension. However, many applications of the smeared-transition scenario are actually in higher-dimensional systems. It is thus useful to discuss what changes in higher dimensions. The most important insight is that the smearing of the transition is driven by the freezing of individual *finite-size* regions of the sample. This implies that the space dimensionality does not play an important role. We thus expect that the same smeared-transition scenario applies in all dimensions. To test this numerically, one could map the d-dimensional dissipative random transverse-field Ising model to a $(d+1)$-dimensional version of the classical Hamiltonian (3.7) and then apply the methods of this paper. Generalizations to other types of dissipation (subohmic and superohmic) are also straight forward, they simply lead to different power-laws in the long-range interaction in the classical Hamiltonian (3.7). The Luijten-Blöte algorithm [120] can be applied in all of these cases.

The most important experimental realizations of smeared quantum phase transitions can arguably be found in disordered metallic magnets. The standard approach to magnetic quantum phase transitions in Fermi liquids [17, 21] leads to an order-parameter field theory with a structure similar to our classical Hamiltonian (3.7). In particular, the order-parameter fluctuations experience Ohmic damping reflected in a long-range $1/\tau^2$ interaction in the imaginary time direction. Recently, indications of frozen local clusters have been observed [122, 123] near the ferromagnetic quantum phase transition in $Ni_{1-x}V_x$. Moreover, the ferromagnetic quantum phase transition in $Sr_{1-x}Ca_xRuO_3$ was shown to be smeared by the disorder introduced via the Ca substitution. [124]

5. ACKNOWLEDGEMENTS

We acknowledge useful discussions with José Hoyos. This work has been supported in part by the NSF under grant nos. DMR-1205803 and PHYS-1066293 as well as the hospitality of the Aspen Center for Physics.

SECTION

2. SUMMARY AND OUTLOOK

This thesis represents a study of the effects of dissipation and disorder in systems undergoing quantum phase transitions. The existence of disorder can change the order of a phase transition from first-order to continuous, and it can also modify the critical behavior, resulting in a different universality class. Dissipation alone can cause a finite-size (zero-dimensional) quantum system to undergo a transition. The addition of dissipation to extended systems can change the universality class of the phase transition. If disorder and dissipation exist simultaneously, stronger effects can be expected. In some cases, these effects can destroy the phase transition by smearing.

Dissipation and disorder play important roles for quantum phase transitions in metallic systems. For example, an extremely thin nanowire made of MoGe undergoes a quantum phase transition from a metallic to a superconducting state as a function of its thickness. The disorder arises from random positions of the magnetic impurities on the surface which are believed to destroy the superconducting order, and the dissipation is caused by conduction electrons. In $Sr_{1-x}Ca_xRuO_3$, the sharp ferromagnetic to paramagnetic quantum phase transition driven by the composition x is completely destroyed by the dissipation due to conduction electrons and the disorder introduced via the Ca substitution.

The first part of this thesis consists of a brief introduction into the field of phase transitions, disorder, and percolation. The original research reported thereafter addressed three specific questions within the field of disordered quantum phase

transitions. In paper I, we investigated the quantum critical behavior of a large-N quantum rotor coupled to a subohmic bosonic bath. This model was solved exactly. With increasing dissipation strength, the system undergoes a quantum phase transition from a delocalized phase to a localized phase. The critical exponents of the sub-Ohmic quantum rotor are identical to those of the one-dimensional classical Heisenberg chain with long-range interactions. Thus, the quantum-to-classical mapping is valid for this model.

Paper II studied the influence of sub-Ohmic dissipation on randomly diluted quantum Ising and rotor models. We found that the system undergoes a quantum phase transition across the percolation threshold from an unusual super-paramagnetic cluster phase to an inhomogeneous ferromagnetic phase as the dilution p increases. We related our results to the smeared transition scenario for disordered quantum phase transitions.

In the last paper, we used Monte-Carlo simulations to study the influences of Ohmic dissipation on the random transverse-field Ising chain. We applied the highly efficient cluster algorithm proposed by Luijten and Blöte to implement the large-range interactions in time which stem from integrating out the modes of the dissipative bath. Our results provide numerical evidence for the predictions of a recent strong-disorder renormalization group theory. In particular, the simulations confirm that the combined effects of disorder and dissipation lead to a destruction of the sharp quantum phase transition by smearing. This happens because different spatial regions can undergo the phase transition independently of the bulk system at different values of the tuning parameter.

Our large-scale Monte Carlo simulation was performed for a one-dimensional random transverse-field Ising model with Ohmic dissipation to study the smearing of the phase transition. However, many applications of the smeared-transition scenario are actually in two and three-dimensional systems. It is thus important to study what changes in higher dimensions.

Moreover, in our investigations of the quantum-to-classical mapping, we have focused on systems without the Berry phase term in the action. This leads to the important question of whether Berry phase effects might invalidate the quantum-to-classical mapping. Answering these questions remains a task for the future.

BIBLIOGRAPHY

[1] S. L. Sondhi, S. M. Girvin, J. P. Carini, and D. Shahar. *Rev. Mod. Phys.*, 69:315, 1997.

[2] S. Sachdev. *Physics World*, 12(4):33, 1999.

[3] S. Sachdev. *Quantum phase transitions*. Cambridge University Press, Cambridge, 1999.

[4] T. Vojta. *Ann. Phys. (Leipzig)*, 9:403, 2000.

[5] M. Vojta. *Rep. Progr. Phys.*, 66:2069, 2003.

[6] L. D. Landau. *Phys. Z. Sowjetunion*, 11:26, 1937.

[7] L. D. Landau. *Zh. Eksp. Teor. Fiz.*, 7:19, 1937.

[8] L. D. Landau. *Phys. Z. Sowjetunion*, 11:545, 1937.

[9] L. D. Landau. *Zh. Eksp. Teor. Fiz.*, 7:627, 1937.

[10] L. Onsager. *Phys. Rev.*, 65:117–149, 1944.

[11] L. P. Kadanoff. *Statistical physics: Statics, dynamics and renormalization*. World Scientic, Singapore, 2000.

[12] C. Domb. *The Critical Point: A Historical Introduction to the Modern Theory of Critical Phenomena*. Taylor & Francis, London, 1996.

[13] B. Widom. *J. Chem. Phys.*, 43:3892, 1965.

[14] N. Goldenfeld. *Lectures on phase transitions and the renormalization group*. Addison-Wesley, Reading, 1992.

[15] M. Kardar. *Statistical physics of fields*. 2007.

[16] L. P. Kadanoff, W. Götze, D. Hamblen, R. Hecht, E. A. S. Lewis, V. V. PALCIAUSKAS, M. RAYL, and J. SWIF. *Rev. Mod. Phys.*, 39:395, 1967.

[17] J. Hertz. *Phys. Rev. B*, 14:1165, 1976.

[18] H. V. Löhneysen, T. Pietrus, G. Portisch, H. G. Schlager, A. Schörder, M. Sieck, and T. Trappmann. *Phys. Rev. Lett.*, 72:3262, 1994.

[19] H. von Löhneysen, A. Rosch, M. Vojta, and P. Wölfle. *Rev. Mod. Phys.*, 79:1015, 2007.

[20] S. Chakravarty, B. I. Halperin, and D. R. Nelson. *Phys. Rev. B*, 39:2344, 1989.

[21] A. J. Millis. *Phys. Rev. B*, 48:7183, 1993.

[22] M. Suzuki. *Progr. Theor. Phys.*, 56:1454, 1976.

[23] M. Suzuki. *Commun. Math. Phys.*, 51:183, 1976.

[24] A. C. Hewson. *The Kondo Problem to Heavy Fermions*. Cambridge University Press, Cambridge, 1993.

[25] P. W. Anderson, G. Yuval, and D. R. Hamann. *Phys. Rev. B*, 1:4464, 1970.

[26] D. Withoff and E. Fradkin. *Phys. Rev. Lett.*, 64:1835, 1990.

[27] A. J. Leggett, S. Chakravarty, A. T. Dorsey, M. P. A. Fisher, A. Garg, and W. Zwerger. *Rev. Mod. Phys.*, 59:1, 1987.

[28] U. Weiss. *Quantum disspative systems*. World Scientific, Singapore, 1993.

[29] R. Bullaand N.-H. Tong and M. Vojta. *Phys. Rev. Lett.*, 91:170601, 2003.

[30] T. Vojta. *J. Phys. A*, 39:R143, 2006.

[31] T. Vojta. *J. Low Temp. Phys.*, 161:299, 2010.

[32] M. E. Fisher. *Phys. Rev.*, 180:594, 1969.

[33] A. B. Harris. *J. Phys. C*, 7:1671, 1974.

[34] G. Grinstein. In E. G. D. Cohen, editor, *Fundamental Problems in Statistical Mechanics VI*, page 147. Elsevier, New York, 1985.

[35] O. Motrunich, S. C. Mau, D. A. Huse, and D. S. Fisher. *Phys. Rev. B*, 61:1160, 2000.

[36] C. Holm and W. Janke. *Phys. Rev. B*, 48:936, 1993.

[37] A. M. Ferrenberg and D. P. Landau. *Phys. Rev. B*, 44:5081, 1991.

[38] H. G. Ballesteros, L. A. Fernandez, V. Martin-Mayor, A. Munoz Sudupe, G. Parisi, and J. J. Ruiz-Lorenzo. *Phys. Rev. B*, 58:2740, 1998.

[39] D. S. Fisher. *Phys. Rev. Lett.*, 69:534, 1992.

[40] D. S. Fisher. *Phys. Rev. B*, 51:6411, 1995.

[41] B. M. McCoy and T. T. Wu. *Phys. Rev. Lett.*, 21:549, 1968.

[42] B. M. McCoy and T. T. Wu. *Phys. Rev.*, 176:631, 1968.

[43] S. Huether, R. Kinney, and T. Vojta. *Phys. Rev. B*, 74:094425, 2006.

[44] R. Sknepnek and T. Vojta. *Phys. Rev. B*, 69:174410, 2004.

[45] T. Vojta. *J. Phys. A*, 36:10921, 2003.

[46] T. Vojta. *Phys. Rev. Lett.*, 90:107202, 2003.

[47] J. A. Hoyos and T. Vojta. *Phys. Rev. Lett.*, 100:240601, 2008.

[48] J. A. Hoyos and T. Vojta. *Physica E*, 42:383–387, 2010.

[49] J. Fröhlich and T. Spencer. *Commun. Math. Phys.*, 84:87, 1982.

[50] E. Bayong, H. T. Diep, and T. T. Truong. *J. Appl. Phys.*, 85:6088, 1999.

[51] S. A. Cannas. *Phys. Rev. B*, 52:3034, 1995.

[52] Daniel W. Strook. *Probability Theory: An Analytic View*. Cambridge University Press, Cambridge, 2010.

[53] D. Stauffer and A. Aharony. *Introduction to Percolation Theory*. CRC Press, Boca Raton, 1991.

[54] A. B. Harris. *J. Phys. C*, 7:3082, 1974.

[55] R.B. Stinchcombe. *J. Phys. C*, 14:L263, 1981.

[56] R. R. dos Santos. *J. Phys. C*, 15:3141, 1982.

[57] T. Senthil and S. Sachdev. *Phys. Rev. Lett.*, 77:5292, 1996.

[58] P. Coleman and A. J. Schofield. *Nature*, 433:226, 2005.

[59] P. Gegenwart, Q. Si, and F. Steglich. *Nature Physics*, 4:186, 2008.

[60] S. Sachdev. *Nature Physics*, 4:173, 2008.

[61] M. Vojta. *Phil. Mag.*, 86:1807, 2006.

[62] P. W. Anderson, G. Yuval, and D. R. Hamann. *Phys. Rev. B*, 1:4464–4473, Jun 1970.

[63] M. Vojta, N.-H. Tong, and R. Bulla. *Phys. Rev. Lett.*, 94:070604, 2005.

[64] A. Winter, H. Rieger, M. Vojta, and R. Bulla. *Phys. Rev. Lett.*, 102:030601, 2009.

[65] A. Alvermann and H. Fehske. *Phys. Rev. Lett.*, 102:050601, 2009.

[66] M. Vojta, R. Bulla, F. Güttge, and A. Anders. *Phys. Rev. B*, 81:075122, 2010.

[67] N.-H. Tong and Y.-H. Hou. 2010. arXiv:1012:5615.

[68] Stefan Kirchner. *J. Low Temp. Phys.*, 161:282–298, 2010.

[69] Matthew T. Glossop and Kevin Ingersent. *Phys. Rev. Lett.*, 95:067202, Aug 2005.

[70] Stefan Kirchner, Qimiao Si, and Kevin Ingersent. *Phys. Rev. Lett.*, 102:166405, Apr 2009.

[71] Mengxing Cheng, Matthew T. Glossop, and Kevin Ingersent. *Phys. Rev. B*, 80:165113, Oct 2009.

[72] Subir Sachdev, Chiranjeeb Buragohain, and Matthias Vojta. *Science*, 286(5449):2479–2482, 1999.

[73] Lijun Zhu, Stefan Kirchner, Qimiao Si, and Antoine Georges. *Phys. Rev. Lett.*, 93:267201, Dec 2004.

[74] L. F. Cugliandolo, D. R. Grempel, G. Lozano, H. Lozza, , and C. A. da Silva Santos. *Phys. Rev. B*, 66:094404, 2002.

[75] Scott Drewes, Daniel P. Arovas, and Scot Renn. *Phys. Rev. B*, 68:165345, Oct 2003.

[76] G. S. Joyce. *Phys. Rev.*, 146:349–358, Jun 1966.

[77] Thomas Vojta. *Phys. Rev. B*, 53:710–714, Jan 1996.

[78] Thomas Vojta and Michael Schreiber. *Phys. Rev. B*, 53:8211–8214, Apr 1996.

[79] R. P. Feynman and A. R. Hibbs. *Quantum Mechanics and Path Integrals*. McGraw-Hill, New York, 1965.

[80] G. W. Ford, J. T. Lewis, and R. F. O'Connell. *Phys. Rev. Lett.*, 55:2273–2276, Nov 1985.

[81] G. W. Ford, J. T. Lewis, and R. F. O'Connell. *Ann. Phys. (N.Y.)*, 185:270, Nov 1988.

[82] T. H. Berlin and M. Kac. *Phys. Rev.*, 86:821–835, Jun 1952.

[83] M. E. Fisher, S.-K. Ma, and B. G. Nickel. *Phys. Rev. Lett.*, 29:917, 1972.

[84] Masuo Suzuki. *Progress of Theoretical Physics*, 49(2):424–441, 1973.

[85] Masuo Suzuki. *Progress of Theoretical Physics*, 49(4):1106–1120, 1973.

[86] M. Thill and D. A. Huse. *Physica A*, 214:321, 1995.

[87] A. P. Young and H. Rieger. *Phys. Rev. B*, 53:8486, 1996.

[88] T. Vojta and J. A. Hoyos. Quantum phase transitions on percolating lattices. In J. Boronat, G. Astrakharchik, and F. Mazzanti, editors, *Recent Progress in Many-Body Theories*, page 235. World Scientific, Singapore, 2008.

[89] T. Senthil and S. Sachdev. *Phys. Rev. Lett.*, 77:5292, 1996.

[90] Rafael M. Fernandes and Jörg Schmalian. *Phys. Rev. Lett.*, 106(6):067004, Feb 2011.

[91] T. Vojta and J. Schmalian. *Phys. Rev. B*, 72:045438, 2005.

[92] T. Vojta and R. Sknepnek. *Phys. Rev. B.*, 74:094415, 2006.

[93] L. Wang and A. W. Sandvik. *Phys. Rev. Lett.*, 97:117204, 2006.

[94] Ling Wang and Anders W. Sandvik. *Phys. Rev. B*, 81(5):054417, Feb 2010.

[95] A. J. Millis, D. K. Morr, and J. Schmalian. *Phys. Rev. Lett.*, 87:167202, 2001.

[96] G. Schehr and H. Rieger. *Phys. Rev. Lett.*, 96:227201, 2006.

[97] G. Schehr and H. Rieger. *J. Stat. Mech.*, page P04012, 2008.

[98] J. A. Hoyos and T. Vojta. *Phys. Rev. B*, 85:174403, 2012.

[99] J. A. Hoyos, C. Kotabage, and T. Vojta. *Phys. Rev. Lett.*, 99:230601, 2007.

[100] Adrian Del Maestro, Bernd Rosenow, Markus Müller, and Subir Sachdev. *Phys. Rev. Lett.*, 101:035701, 2008.

[101] T. Vojta, C. Kotabage, and J. A. Hoyos. *Phys. Rev. B*, 79:024401, 2009.

[102] T. Vojta, J. A. Hoyos, P. Mohan, and R. Narayanan. *Journal of Physics: Condensed Matter*, 23:094206, 2011.

[103] J. A. Hoyos and T. Vojta. *Phys. Rev. B*, 74:140401(R), 2006.

[104] L. F. Cugliandolo, G. S. Lozano, and H. Lozza. *Phys. Rev. B*, 71:224421, 2005.

[105] N. V. Prokofev and P. C. E. Stamp. *Rep. Progr. Phys.*, 63:669, 2000.

[106] I. Chiorescu, W. Wernsdorfer, A. Müller, H. Bögge, and B. Barbara. *Phys. Rev. Lett.*, 84:3454, 2000.

[107] W. Wernsdorfer. *Adv. Chem. Phys.*, 118:99, 2001.

[108] Jürg Fröhlich, Robert Israel, Elliot H. Lieb, and Barry Simon. *Commun. Math. Phys.*, 62:1–34, 1978.

[109] T. Vojta and J. Schmalian. *Phys. Rev. Lett.*, 95:237206, 2005.

[110] Manal Al-Ali and Thomas Vojta. *Phys. Rev. B*, 84:195136, Nov 2011.

[111] J. Sak. *Phys. Rev. B*, 15:4344–4347, May 1977.

[112] E. Luijten and H. W. J. Blöte. *Phys. Rev. Lett*, 89:025703, 2002.

[113] P. Werner, K. Völker, M. Troyer, and S. Chakravarty. *Phys. Rev. Lett.*, 94:047201, 2005.

[114] Y. Imry and M. Wortis. *Phys. Rev. B*, 19:3580, 1979.

[115] Kenneth Hui and A. Nihat Berker. *Phys. Rev. Lett.*, 62:2507, 1989.

[116] M. Aizenman and J. Wehr. *Phys. Rev. Lett.*, 62:2503, 1989.

[117] R. Greenblatt, M. Aizenman, and J. Lebowitz. *Phys. Rev. Lett.*, 103:197201, 2009.

[118] H. Rieger and A. P. Young. *Phys. Rev. B*, 54:3328, 1996.

[119] U. Wolff. *Phys. Rev. Lett.*, 62:361, 1989.

[120] E. Luijten and H. W. J. Blöte. *Int. J. Mod. Phys. C*, 6:359, 1995.

[121] F. Hrahsheh, H. Barghathi, and T. Vojta. *J. Phys. B*, 84:184202, 2011.

[122] S. Ubaid-Kassis, T. Vojta, and A. Schroeder. *Phys. Rev. Lett.*, 104:066402, 2010.

[123] A. Schroeder, S. Ubaid-Kassis, and T. Vojta. *J. Phys. Condens. Matter*, 23:094205, 2011.

[124] L. Demkó, S. Bordács, T. Vojta, D. Nozadze, F. Hrahsheh, C. Svoboda, B. Dóra, H. Yamada, M. Kawasaki, Y. Tokura, and I. Kézsmárki. *Phys. Rev. Lett.*, 108:185701, 2012.

VITA

Manal Al-Ali was born on October 06, 1983 in Irbid , Jordan. She finished her elementary and secondary school in Huson Camp, Irbid. She received her bachelor degree in Physics from Yarmouk University in 2005. While she was working as a teacher in the Jordan Ministry of Education, she joined the group of Dr. A. Obeidat as a graduate student in the department of Physics at Jordan University of Science and Technology (JUST). In August 2009, she received her MS in theoretical Physics from JUST. In January 2010, she moved to Missouri University of Science and Technology (Missouri S&T) in Rolla-USA to join the group of Dr. Thomas Vojta until she earned her PhD degree in Physics in the December of 2013.